Journal of Colloid and Interface Science 500 (2017) 182–201

Contents lists available at ScienceDirect

Journal of Colloid and Interface Science

journal homepage: www.elsevier.com/locate/jcis

Feature Article

Particle manipulations in non-Newtonian microfluidics: A review

Xinyu Lu [a], Chao Liu [b], Guoqing Hu [b], Xiangchun Xuan [a,*]

[a] Department of Mechanical Engineering, Clemson University, Clemson, SC 29634-0921, USA
[b] State Key Laboratory of Nonlinear Mechanics, Beijing Key Laboratory of Engineered Construction and Mechanobiology, Institute of Mechanics, Chinese Academy of Sciences, Beijing 100190, China

GRAPHICAL ABSTRACT

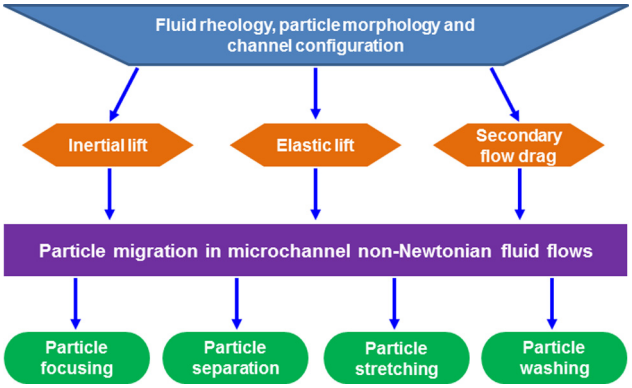

ARTICLE INFO

Article history:
Received 31 January 2017
Revised 26 March 2017
Accepted 6 April 2017
Available online 8 April 2017

Keywords:
Elastic lift
Inertial lift
Particle focusing
Particle separation
Particle washing
Particle stretching

ABSTRACT

Microfluidic devices have been widely used since 1990s for diverse manipulations of particles (a general term of beads, cells, vesicles, drops, etc.) in a variety of applications. Compared to the active manipulation via an externally imposed force field, the passive manipulation of particles exploits the flow-induced intrinsic lift and/or drag to control particle motion with several advantages. Along this direction, inertial microfluidics has received tremendous interest in the past decade due to its capability to handle a large volume of samples at a high throughput. This inertial lift-based approach in Newtonian fluids, however, becomes ineffective and even fails for small particles and/or at low flow rates. Recent studies have demonstrated the potential of elastic lift in non-Newtonian fluids for manipulating particles with a much smaller size and over a much wider range of flow rates. The aim of this article is to provide an overview of the various passive manipulations, including focusing, separation, washing and stretching, of particles that have thus far been demonstrated in non-Newtonian microfluidics.

Contents

* Corresponding author.
E-mail address: xcxuan@clemson.edu (X. Xuan).

http://dx.doi.org/10.1016/j.jcis.2017.04.019
0021-9797/

1. Introduction

Microfluidic devices have been widely used over the past two decades for diverse manipulations of particles (a general term of beads, cells, vesicles, drops, etc.) such as focusing [1,2], trapping/concentration [3,4] and separation [5,6] in a variety of chemical, environmental and biomedical applications. They possess a number of advantages over their macroscopic counterparts such as increased efficiency, portability and environmental compatibility at a reduced cost of samples and operation [7,8]. However, the majority of these devices have been tested with only particles suspended in aqueous buffer solutions that are Newtonian fluids with a constant viscosity. As a matter of fact, many of the real chemical (e.g., colloidal suspensions and polymer solutions) [9,10] and biological (e.g., blood, saliva and DNA solutions) [11,12] samples exhibit non-Newtonian characteristics such as shear thinning and viscoelasticity [13,14]. Hence, there has recently been an growing interest in the fundamental and application studies of microfluidic particle manipulations in non-Newtonian fluids [15,16].

Compared to the active manipulation of particles via an externally imposed force field (e.g., acoustic [17], electric [18], magnetic [19] or optical [20]), the passive manipulation exploits the flow-induced intrinsic lift and/or drag force to control particle motion with several advantages such as simplicity and autonomy [21]. Along this direction, inertial microfluidics has attracted tremendous attention since the pioneering study of Di Carlo et al. [22] due to its capability to handle a large volume of samples at a high throughput [23,24]. This inertial lift-based approach in Newtonian fluids, however, becomes ineffective and even fails for small particles and/or at low flow rates where the particle Reynolds number becomes much smaller than 1 [25]. Recent studies have demonstrated the potential of elastic lift in non-Newtonian fluids for manipulating particles with a much smaller size [26–28] and over a much wider range of flow rates [29] than in Newtonian fluids. Moreover, the combination of elastic lift with inertial lift can greatly enhance the particle control in microchannels at increasing flow rates [30,31].

The aim of this article is to provide an overview of the diverse applications of the flow-induced lift and/or drag force to passive particle manipulations in non-Newtonian microfluidic devices. The fundamental investigations of particle motions in non-Newtonian fluids, including the sedimentation in stationary fluids and the cross-stream migration in flowing fluids, are not discussed here. The readers are suggested to refer to the review articles from Leal [32,33] and Brunn [34] as well as the book chapter from McKinley [35] for those early-date studies of particle motions in stationary non-Newtonian fluids and in non-Newtonian fluid flows through cylindrical pipes with a diameter of the order of few millimeters. The readers are also suggested to refer to the review articles from D'Avino & Maffettone [15] and D'Avino et al. [16] for the recent advancements in the fundamental understanding (primarily numerical [e.g., 36–42]) of particle motions in non-Newtonian fluid flows through straight microchannels of various shapes.

This article is organized as follows. Section 2 presents a brief background of the common non-Newtonian fluids and the flow induced lift and drag forces as well as the non-dimensional numbers that are often defined for particle transport and manipulations in microchannel non-Newtonian fluid flows. Section 3 reviews the particle focusing phenomena in the flow of viscoelastic fluids through straight cylindrical and rectangular microchannels as well as rectangular microchannels with curved fluid streamlines. Section 4 reviews the sheath-focusing and sheath-free approaches to continuous particle separation in viscoelastic fluid flows based on the difference in particle size, shape or deformability. Also reviewed are the hybrid approaches that integrate passive viscoelastic focusing and active magnetic deflection to separate particles based on particle magnetization and/or size. Section 5 reviews a couple of other particle manipulations including washing and stretching in non-Newtonian fluids that are enabled by the cross-stream migration and focusing in microchannel flows. Section 6 concludes the article with some perspectives on future research directions in the field.

2. Background

2.1. Non-Newtonian fluids

Many biological and chemical fluids possess non-Newtonian characteristics [43], where the former include blood [44–46],

plasma [47], saliva [48,49], hyaluronic acid (HA) [50,51] and DNA solutions [52,53], etc. With high-concentration blood cells, blood exhibits viscoelastic and shear-thinning effects due mostly to the highly deformable and elastic properties of red blood cells (RBCs) as well as their reversible aggregations under shear strain [44–46]. With blood cells being removed, liquid plasma still displays a weak viscoelastic effect due to the presence of rich biomolecules (e.g., proteins and glucose) while its viscosity remains nearly constant in a wide range of shear rates [47]. Saliva is an aqueous mixture of high molecular-weight mucins and other biomolecules that both contribute to the fluid viscoelasticity and shear-thinning [48,49]. To date, the only naturally occurring solutions that have been used for studies of particle motion in non-Newtonian microfluidics are HA and DNA solutions. HA is found in many biological systems such as synovial fluids in joints for the prevention of high-load impacts [50]. DNA solution is strongly viscoelastic because of the long relaxation time of DNA molecules [54].

Non-Newtonian chemical fluids are usually made of synthetic polymer powders, which are less expensive and have more stable rheological properties than biofluids [55,56]. The most-often used ones in academic research include polyvinylpyrrolidone (PVP), polyethylene oxide (PEO) and polyacrylamide (PAA) solutions, which are all biocompatible and have been extensively used in microfluidic devices [57,58]. They are prepared in water or any aqueous buffer solution (for a further enhanced biocompatibility), whose viscosity can be tuned by being mixed with glycerol (or other chemicals) at different (weight or volume) ratios. Among the three types of common polymers, PVP has a relatively small molecular weight (e.g., 360 kDa) and its solutions can be safely considered as a viscoelastic Boger fluid with a nearly shear rate-independent viscosity [59,60]. PEO has an intermediate molecular weight (e.g., in the range of 1000–4000 kDa), whose solution is strongly viscoelastic with a weak (in the dilute regime, where the PEO concentration is below the overlapping concentration) to mild (in the semi-dilute regime) shear-thinning effect [61–63]. PAA has the largest molecular weight (e.g., 18 MDa) and hence its solution has the strongest viscoelasticity and shear-thinning effects (among the above three polymer solutions) even at relatively low concentrations. Moreover, PAA solution possesses a non-negligible second normal stress difference, which has been demonstrated to produce a secondary flow over the channel cross-section affecting the motion of particles suspended therein [64]. A variety of constitutive models has been developed to describe the flow of polymeric fluids, among which the often used ones are the power-law, Oldroyd-B (OB), Giesekus and Phan-Thien-Tanner (PTT) models. The readers are referred to the two-volume book of Bird et al. [55] and the review article from Bird and Wiest [65] for the various constitutive equations and their merits and shortcomings.

2.2. Non-dimensional numbers

The motion of particles in microchannel non-Newtonian fluid flows is often characterized by the following dimensionless numbers. The inertial effect on fluid and particle motions is measured by the (channel) Reynolds number, Re, and the particle Reynolds number, Re_p, which both compare the inertial force to viscous force,

$$Re = \frac{\rho V D_h}{\eta_0} \tag{1}$$

$$Re_p = \beta^2 Re \tag{2}$$

$$\beta = \frac{d}{D_h} \tag{3}$$

In the above ρ is the fluid density, V is the average fluid velocity, D_h is the channel's hydraulic diameter, η_0 is the zero-shear fluid viscosity, and β is the dimensionless particle blockage ratio with d being the (equivalent) spherical diameter of particles. The viscoelastic effect on fluid and particle motions is measured by the Weissenberg number, Wi, which compares the elastic force to viscous force,

$$Wi = \lambda\dot{\gamma} = \lambda\frac{2V}{D_h} \tag{4}$$

with λ being the relaxation time of the fluid and $\dot{\gamma} = 2V/D_h$ the average fluid shear rate over the channel cross-section. Another often used dimensionless number for viscoelastic effect is the Deborah number, De, which is defined as the ratio of the fluid relaxation time to the characteristic time of an experimental observation (or a numerical simulation) [15,16], t_p, i.e.,

$$De = \frac{\lambda}{t_p} \tag{5}$$

These two numbers are of the same order in magnitude and sometimes deemed interchangeable in the literature [66]. The viscoelastic effect can also be characterized by the elasticity number, El, which is the ratio of the Weissenberg number (or Deborah number) to Reynolds umber, or equivalently the ratio of the elastic force to inertial force, and hence independent of flow kinematics,

$$El = \frac{Wi}{Re} = \frac{2\lambda\eta_0}{\rho D_h^2} \tag{6}$$

2.3. Flow-induced forces

A (viscoelastic) fluid flowing past a particle exerts a force on the particle due to the action of shear stress and pressure on its surface. This force, by tradition, is decomposed into the lift and drag components that are perpendicular and parallel to the flow direction, respectively. It is normally the former force component that drives the cross-stream particle motion enabling the passive manipulation of particles in microchannel flows. For convenience, the lift force induced in a viscoelastic fluid flow is often broken down into the inertial lift, $\boldsymbol{F}_{iL}$ due to fluid inertia, and the elastic lift, $\boldsymbol{F}_{eL}$ due to fluid elasticity, which are both briefly explained below. We will also briefly explain the drag force due to the secondary flow in the channel cross-section that may contribute to particle manipulations in non-Newtonian microfluidic devices.

2.3.1. Inertial lift

The dominant inertial lift has been proved to consist of two opposing components for a neutrally buoyant particle [33,67]. The wall-induced inertial lift, $\mathbf{F}_{iL\_w}$, is a result of the asymmetric distribution of wake vorticity around a near-wall particle, which increases the fluid pressure in the particle-wall gap and hence pushes the particle away from the wall. It decreases with the increasing particle-wall distance and vanishes along the symmetric axis (or plane) of a confined channel [68,69]. The shear gradient-induced inertial lift, $\mathbf{F}_{iL\_s}$, is a result of the curvature of the fluid velocity profile, which directs a particle away from the channel center. It increases from zero at the channel center and gets the largest at the channel wall where the fluid shear rate is the highest [21]. These two inertial lift components act together to lead to equilibrium particle positions in confined channels [23–25]. For example, particles are inertially focused to either an annulus in a straight cylindrical channel that is about 0.6 times the radius from the center [70], or multiple symmetric equilibrium positions in a straight rectangular microchannel that are at the centers of the channel faces [71] and/or near the corners [72].

It has been well accepted in the literature [21–25] that the dominant inertial lift, $\mathbf{F}_{iL} = \mathbf{F}_{iL\_w} + \mathbf{F}_{iL\_s}$, scales as [73]

$$\mathbf{F}_{iL} = C_{iL}\rho d^4\dot{\gamma}^2 \tag{7}$$

where the non-dimensional inertial lift coefficient, C_{iL}, is a function of Reynolds number and the normalized particle position over the channel cross-section. Di Carlo et al. [74] have recently revised the scaling of $\mathbf{F}_{iL}$ for a particle near the wall or the centerline of a straight square microchannel. More recently, Liu et al. [75] have proposed fitting formulae to the direct numerical simulation (DNS) data of $\mathbf{F}_{iL}$ for spheres in straight rectangular microchannels. In general $\mathbf{F}_{iL}$ is found to play an effective role only when the particle Reynolds number reaches the order of 1 [21–25]. Other weaker inertial lift forces that are less studied in the literature include the rotation-induced Magnus force and the slip-induced Saffman force [76–78]. They are usually much smaller than the dominant inertial lift, $\mathbf{F}_{iL}$, unless, for example, a direct-current electric field is imposed to generate a strong electrophoretic slip velocity for pressure-driven particle motion [79].

2.3.2. Elastic lift

The elastic lift, $\mathbf{F}_{eL}$, on a particle results from the non-uniform normal stress differences in viscoelastic fluid flows [80,81]. The first normal stress difference, $N_1 = \tau_{11} - \tau_{22}$, creates an extra tension along fluid streamlines [55]. The second normal stress difference, $N_2 = \tau_{22} - \tau_{33}$, produces a secondary flow over the channel cross-section [82]. In these definitions, the normal stresses, τ_{11}, τ_{22} and τ_{33}, are in the translational direction, velocity gradient direction and rotational direction, respectively. As the magnitude of N_2 is much smaller than that of N_1 for most viscoelastic polymer solutions [83,84], we can use the Oldroyd-B model as a constitutive equation to evaluate N_1 [60],

$$N_1 = -2\eta_p\lambda\dot{\gamma}^2 \tag{8}$$

where η_p is the polymeric contribution to the solution viscosity. Fig. 1 shows the contours of the normalized $\dot{\gamma}^2$ in the cross sections of a cylindrical microchannel [85](a) and a square microchannel [86] (c, note only the upper right quarter is displayed), respectively. The first normal stress difference, N_1, becomes the smallest at the center in the cylindrical channel (Fig. 1a) while at both the center and the four corners in the square-shaped channel (Fig. 1c).

When the magnitude of N_2 is negligible as compared to that of N_1, the lateral flow-induced elastic lift, $\mathbf{F}_{eL}$, can be assumed solely proportional to the variation of N_1 over the size of a particle [87,88], i.e.,

$$\mathbf{F}_{eL} = C_{eL}d^3\nabla N_1 = -2C_{eL}d^3\eta_p\lambda\nabla\dot{\gamma}^2 \tag{9}$$

where C_{eL} is the non-dimensional elastic lift coefficient, and $\mathbf{F}_{eL}$ points toward the region(s) with a smaller shear rate. The cross-sectional vector plots of $-\nabla\dot{\gamma}^2$, which is proportional to ∇N_1 based on Eq. (8), are shown in Fig. 1 for both a cylindrical microchannel (b) and a square microchannel (d, only the upper right quarter is displayed). Therefore, $\mathbf{F}_{eL}$ alone drives the particle toward the centerline in the cylindrical channel or both the centerline and the four corners in the square one. However, as both $\mathbf{F}_{iL}$ in Eq. (7) and $\mathbf{F}_{eL}$ in Eq. (9) are a strong function of flow rate (reflected by the fluid shear rate, $\dot{\gamma}$), the equilibrium particle position will vary with the increase of flow rate or fluid inertia. For example, the corner equilibrium position in a square microchannel has been demonstrated to disappear at an increased flow due to the increasing role of the wall-induced inertial lift [29,30].

2.3.3. Drag

The cross-stream drag force can have a strong impact on the position of moving particles in a viscoelastic fluid flow through a microchannel. It arises from the secondary fluid flow in the channel cross section that may be induced by either the streamline

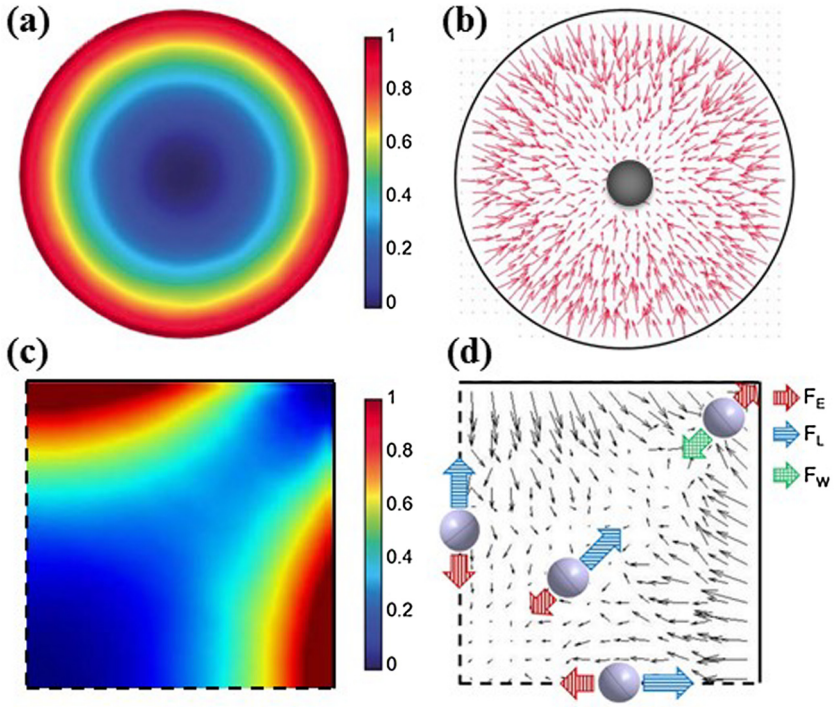

Fig. 1. Cross sectional contours of the shear rate squared, $\dot{\gamma}^2$ (a, c; normalized) and vectors of the induced elastic lift on a particle, $\mathbf{F}_{eL}$ (b, d; in terms of $-\nabla\dot{\gamma}^2$, normalized) in viscoelastic fluid flow through: (a, b) cylindrical microchannel. Adapted with permission from Seo et al. [85], © 2014 The Royal Society of Chemistry; (c, d) a square microchannel (only the upper right quarter is shown). Adapted with permission from Seo et al. [86], © 2014 AIP Publishing LLC. The symbols, F_E, F_L, and F_W in (d) represent the elastic lift, shear-gradient induced inertial lift, and wall-induced inertial lift, respectively, as the flow rate increases.

curvature [89] or the second normal stress difference of the fluid [82]. The former situation occurs in both a curving channel (e.g., serpentine or spiral shaped) and a straight channel with expansions and contractions, where the fluid inertia causes a Dean flow in the form of counter-rotating vortices in the channel cross section [90]. The strength of this flow is often characterized by the Dean number, *Dn*,

$$Dn = Re\sqrt{\frac{D_h}{2R}} \tag{10}$$

where R is the radius of curvature of the path of the channel. In addition, the non-zero second normal stress difference in a strongly elastic fluid (e.g., PAA solution) has been demonstrated to cause a rotational secondary fluid flow in the cross section of even a straight microchannel [64,82]. In either circumstance, however, the secondary flow is usually very weak as compared to the primary fluid flow along the path of the channel, such that the Reynolds number based on the transverse particle migration velocity becomes small. Therefore, the cross-stream drag force, $\mathbf{F}_D$, on a particle, may be safely estimated using Stokes' drag as suggested by Di Carlo et al. [22],

$$\mathbf{F}_D = C_D \frac{\rho V^2 d}{D_h^2 R} \tag{11}$$

where C_D is the non-dimensional Dean drag coefficient.

3. Particle focusing

Particle focusing refers to the alignment of particles into either a two-dimensional (2D) plane or a three-dimensional (3D) line. It is often a necessary step prior to detecting, counting, analyzing and sorting particles for various microfluidic applications such as flow cytometers and continuous-flow sorters [1,2]. It also helps avoiding particle adhesions to microchannel walls for an enhanced recovery rate, which is particularly important to precious samples. There have been numerous particle focusing methods developed in microchannel Newtonian fluid flows, and the readers are suggested to refer to the review papers from, for example, Huh et al. [91], Chung and Kim [92], Godin et al. [93], and Xuan et al. [2]. What follows is a review of the particle focusing phenomena in the flow of non-Newtonian fluids through microchannels of various shapes.

3.1. Straight cylindrical microchannels

As viewed from Fig. 1b, the flow-induced elastic lift directs particles radially inward in a cylindrical channel, leading to eventually a focused particle stream along the centerline. Such a 3D focusing effect was first observed by Karnis et al. for sub-millimeter particles in circular pipes of millimeter-diameter in 1960s [94,95]. It has been demonstrated effective for both micro particles [96] and submicron-sized Brownian particles [27] in cylindrical microchannels. It has also been recently utilized by Dannhauser et al. [97] to align erythrocytes for a continuous characterization of the morphological property of every individual cell. This viscoelastic focusing is affected by several factors including the fluid

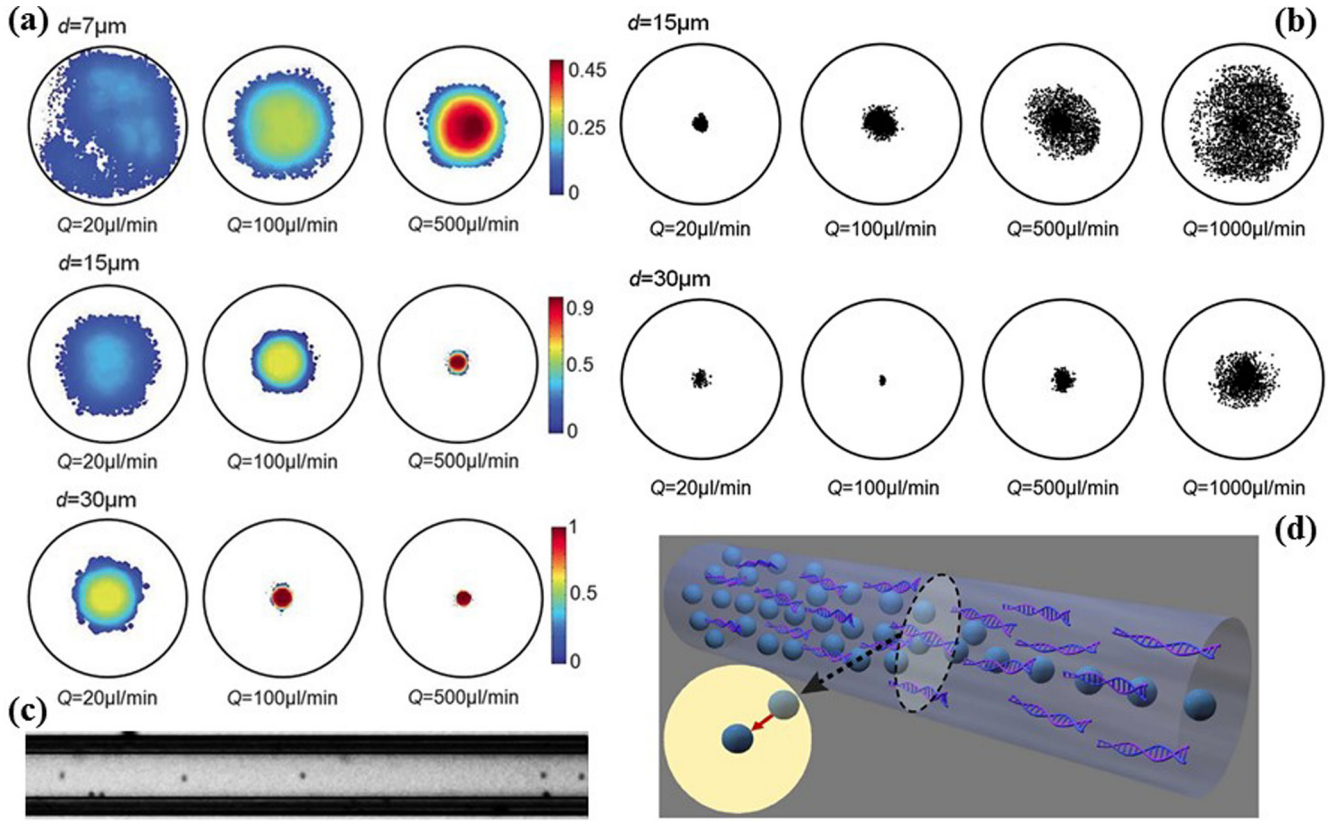

Fig. 2. Viscoelastic particle focusing in cylindrical microchannels. (a) Cross-sectional variation of particle (with three diameters: 7 μm, 15 μm and 30 μm) concentration in a 300 μm-diameter pipe flow of an elasticity-dominant (8% PVP) fluid at different flow rates. (b) Cross-sectional position of particles (with diameters of 15 μm and 30 μm) in a strong shear-thinning fluid (1% PEO) in the same pipe as in (a) at different flow rates. Adapted with permission from Seo et al. [85], © 2014 The Royal Society of Chemistry. (c) Bi-stability focusing of 4 μm diameter particles at the centerline and the wall of a 50 μm diameter cylindrical pipe. Adapted with permission from D'Avino et al. [98], © 2012 The Royal Society of Chemistry. (d) Schematic diagram for particle focusing in a DNA-laden flow through a cylindrical microchannel. Adapted with permission from Kang et al. [96], © 2013 Macmillan Publishers Limited.

rheological properties (Wi), particle blockage ratio (β), flow rate (Re), and channel length etc. Seo et al. [85] measured using a holographic technique the position and concentration of polystyrene (PS) particles in an elasticity-dominant fluid (8% PVP) flow through a 300 μm-diameter circular pipe. The focusing effect at the centerline gets improved significantly for larger particles and at higher flow rates (Fig. 2a). This trend was, however, reversed in 1% PEO solution (4000 kDa molecular weight), where the nearly single-line particle focusing in the same pipe at a low flow rate becomes worse at medium to high flow rates due to the fluid's strong shear-thinning effects (Fig. 2b) [85]. In the latter experiment with the particle Reynolds number, Re_p, being on the order of 0.1, the inertial lift, which alone focuses particles to the annulus of 0.6 times radius of a cylindrical channel [71], may also play a role.

More interestingly, D'Avino et al. [98] observed in the same polymer solution (i.e., 1% PEO) a bi-stability focusing of PS particles at both the centerline and the wall of a cylindrical microchannel when the flow rate is small (Fig. 2c). This phenomenon was also attributed to the substantial shear thinning effects of the suspending solution. In addition, Kang et al. [96] demonstrated an efficient particle focusing phenomenon in an extremely dilute DNA solution (0.0005 (w/v)% or 5 ppm) (Fig. 2d), which arises from the large size and long relaxation time of DNA molecules [52,53]. To estimate the effectiveness of viscoelastic particle focusing in cylindrical pipes, Romeo et al. [99] proposed a dimensionless "focusing" number, Θ, that has origins from early theoretical studies [34,100],

$$\Theta = \frac{1}{2} De \left(1 + C\frac{\Psi_2}{\Psi_1}\right)\beta^2 f(\beta)\frac{L}{R} \tag{12}$$

where De is the Deborah number defined earlier, $C \cong 2$ is a constant, $\Psi_1 = N_1/\dot{\gamma}^2$ and $\Psi_2 = N_2/\dot{\gamma}^2$ are the first and second normal stress difference coefficients [101], and $f(\beta) = A + B\beta^2$ accounts for the particle size (through the particle blockage ratio, β) dependence with $A = 6.6$ and $B = -76$ [99]. The accuracy of this non-dimensional parameter was verified by comparing the calculated particle fractions with the experimental measurements in a cylindrical capillary [99]. A similar "focusing" number was also proposed by Seo et al. [85].

3.2. Straight rectangular microchannels

3.2.1. Slit-like microchannels

The earliest study of particle manipulation in non-Newtonian fluid flows through rectangular microchannels was performed by Leshansky et al. [88], who demonstrated a tunable viscoelastic focusing of particles in a shallow microchannel (45 μm high, 1000 μm wide) in dilute polymer solutions. In such a slit-like channel, the flow becomes essentially 2D with insignificant corner effects, and hence the elastic lift force directs particles toward the midplane (Fig. 3a) [102–104]. The observed lateral migrations are well explained by a simple 2D theory based on scaling arguments for particles of different sizes in both 8% PVP and 45 ppm PAA (mixed with 76 wt.% glycerol) solutions at various flow rates (Fig. 3b) [88]. Seo et al. [102] have recently utilized this 2D viscoelastic focusing to place RBCs in phosphate buffered saline (PBS)-based 3% PVP solution to the focal plane of a holographic microscope for quantitative phase imaging. Moreover, as schematically shown in Fig. 3c, the moment of the elastic lift forces from the top and bottom walls of the microchannel re-orient RBCs to

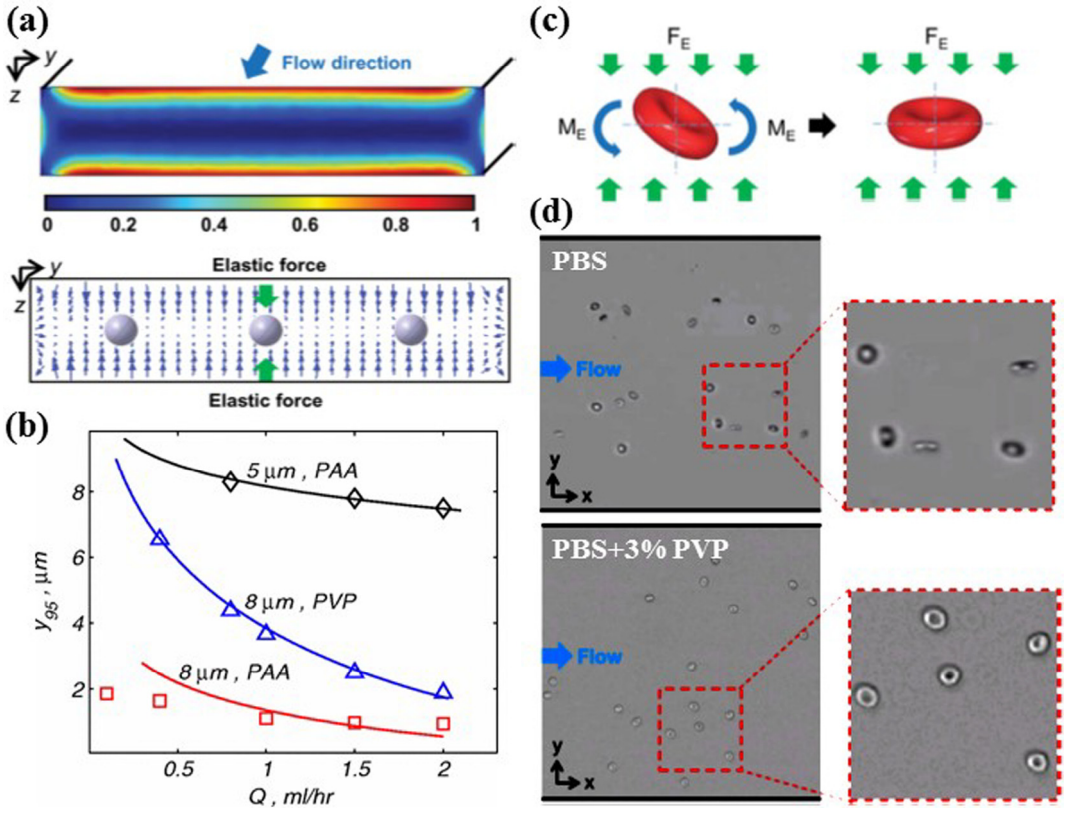

Fig. 3. Viscoelastic particle focusing in slit-like microchannels. (a) Cross sectional contours of the shear rate squared, $\dot{\gamma}^2$ (top, normalized) and vectors of the induced elastic lift force on particles (bottom) in viscoelastic fluid flows. Adapted with permission from Seo et al. [102], © 2014 AIP Publishing LLC. (b) Comparison between the experimental results (void symbols) and the theoretical predictions (solid curves) for viscoelastic particle focusing in dilute polymer solutions. Adapted with permission from Leshansky et al. [88], © 2007 The American Physics Society. (c) Schematic illustrating the re-orientation of RBCs due to the actions of the flow-induced elastic force, $\mathbf{F}_E$, and moment, $\mathbf{M}_E$ [102]. (d) Comparison of the recorded RBC images in the flows of PBS and PBS-based 3% PVP solutions via holographic microscopy [102].

align their major axis with the flow (Fig. 3d). In both experiments, Re_p is so small that the inertial effects are negligible.

3.2.2. Square microchannels

3.2.2.1. Polymer fluids. Particle focusing in polymer fluid flows through straight square microchannels has thus far been studied the most in the literature. Yang et al. [30] proposed the concept of elasto-inertial particle focusing, which, as viewed schematically in Fig. 4a, integrates inertial focusing (i.e., $Re > 0$ and $Wi \approx 0$) and elastic focusing (i.e., $Re \approx 0$ and $Wi > 0$) to align particles in viscoelastic fluid flows along the centerline of a straight microchannel at $Re > 0$ and $Wi > 0$. This sheathless particle focusing technique was demonstrated by the authors [30] using 5.9 μm diameter PS particles in the flow of 500 ppm PEO solution through a 50 μm wide square microchannel. As illustrated in Fig. 4b, the equilibrium particle positions in this mildly elastic fluid (with the elasticity number, $El = 21.51$) are located at the channel center and corners at low flow rates. They reduce to one single stream along the centerline at the flow rate of 0.20 ml/h ($Re = 0.37$ and $Wi = 8.04$) that then spreads out at even higher flow rates due to the increasing inertial effects. A similar trend was also reported in the paper from Del Giudice et al. [105], where a flow rate-enhanced centerline focusing was observed for 10 μm diameter particles in a PVP solution with $El = 49$ through a 50 μm wide square microchannel. Moreover, the measured particle fractions in different concentric bands of the channel cross section can be rescaled to a master curve by the use of the dimensionless focusing number, Θ in Eq. (12), that was originally derived for cylindrical channels [99].

However, the elasto-inertial particle focusing does not work very well if the suspending fluid has either a strong elasticity or a strong shear thinning effect. Yang et al. [30] reported that particles have multiple equilibrium positions in a strongly elastic PVP solution (8% with the elasticity number, $El = 258$) over a wide range of flow rates (Fig. 4c). This observation is consistent with that of Seo et al. [86] in the same fluid. Del Giudice et al. [106] found that in a strongly shear-thinning PEO (1.6%) solution the equilibrium particle position shifts from the centerline toward the four corners at the increasing flow rate (Fig. 4d). Seo et al. [86] also found a significantly weakened particle focusing efficiency in 1% PEO solution. A comprehensive parametric study of the fluid rheology effects on elasto-inertial particle focusing has been recently reported by Song et al. [107] in terms of three dimensionless numbers (*Re*, *Wi*, and *El*). Another work worthy of notice is from Kim et al. [26], who demonstrated a strong viscoelastic focusing of submicron particles in 500 ppm PEO solution toward multiple equilibrium positions in a 5 μm wide square channel (Fig. 4e). This work indicates the potential to elastically focus bacterial cells, which are usually too small to be effectively manipulated with fluid inertia, in straight microchannels.

3.2.2.2. Biofluids. Viscoelastic particle focusing has also been demonstrated in biofluids including DNA and HA solutions. DNA molecules usually have a much longer relaxation time than synthetic polymers due to their structural rigidity. DNA solutions are therefore more elastic and able to sustain an effective particle focusing at higher flow rates than in polymer solutions. They are also strongly shear thinning unless the DNA concentration is very low (≤10 ppm) as viewed from the plot of viscosity vs. shear rate in Fig. 5a [108]. Fig. 5b shows the experimental images of a heterogeneous three-particle mixture in 5 ppm λ-DNA solution at a range of flow rates. The equilibrium particle positions are found to experience a similar shifting to those in polymer solutions with increasing flow rates [30], i.e., from multiple at the centerline and four corners to one at the centerline that then dispersed. In another study Lim et al. [29] demonstrated an extremely high-throughput particle focusing in the flow of weakly elastic HA solutions. They

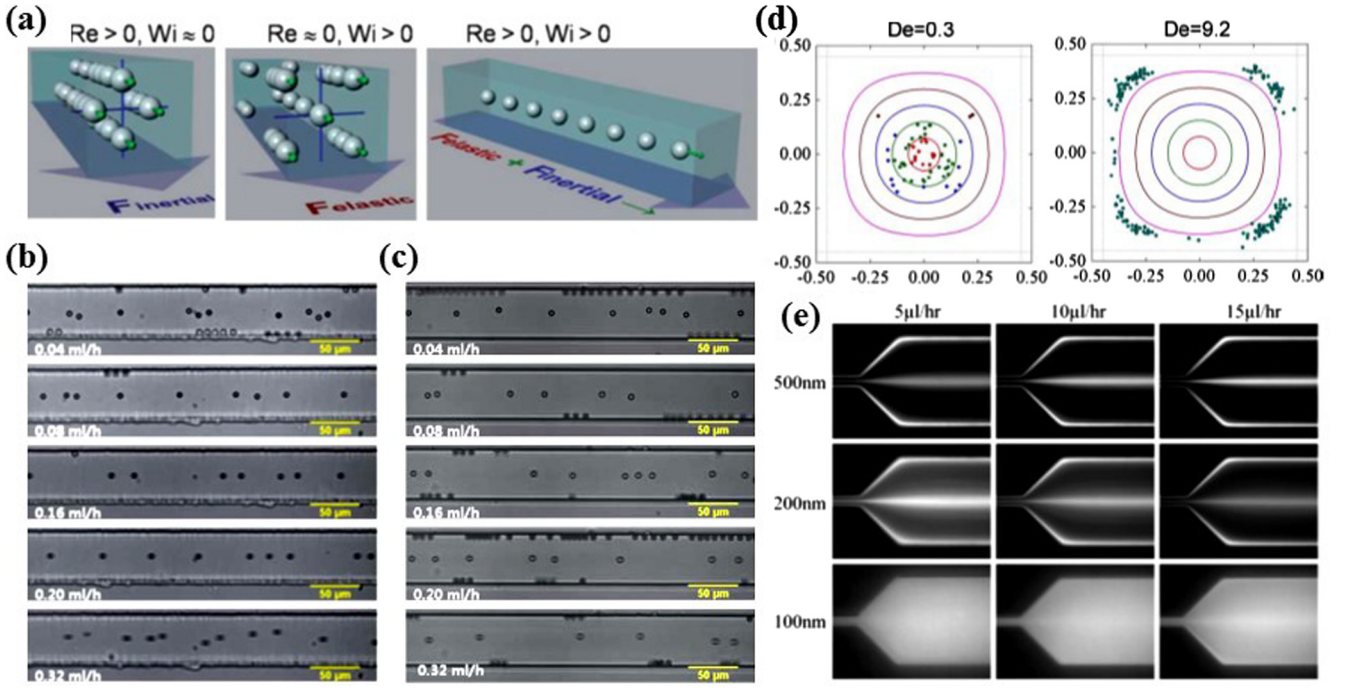

Fig. 4. Particle focusing in polymer fluid flows through straight square microchannels. (a) Schematic illustration of elasto-inertial particle focusing that integrates inertial and elastic effects in a viscoelastic fluid. Adapted with permission from Yang et al. [30], © 2011 The Royal Society of Chemistry. (b, c) Top-view images of 5.9 μm diameter particles in the flows of 500 ppm PEO solution (b) and 8% PVP solution (c), respectively, through a 50 μm wide square channel [30]. (d) Cross-sectional positions of 10 μm diameter particles in 1.6% PEO solution through a 100 μm wide square microchannel at the flow rates of 0.1 μl/min (with the Deborah number, $De = 0.3$) and 3 μl/min ($De = 0.3$), respectively. Adapted with permission from Del Giudice et al. [106], © 2015 Springer. (e) Distributions of submicron PS particles in 500 ppm PEO solution at the outlet of a 4 cm long and 5 μm wide straight square microchannel. Adapted with permission from Kim et al. [26], © 2012 The Royal Society of Chemistry.

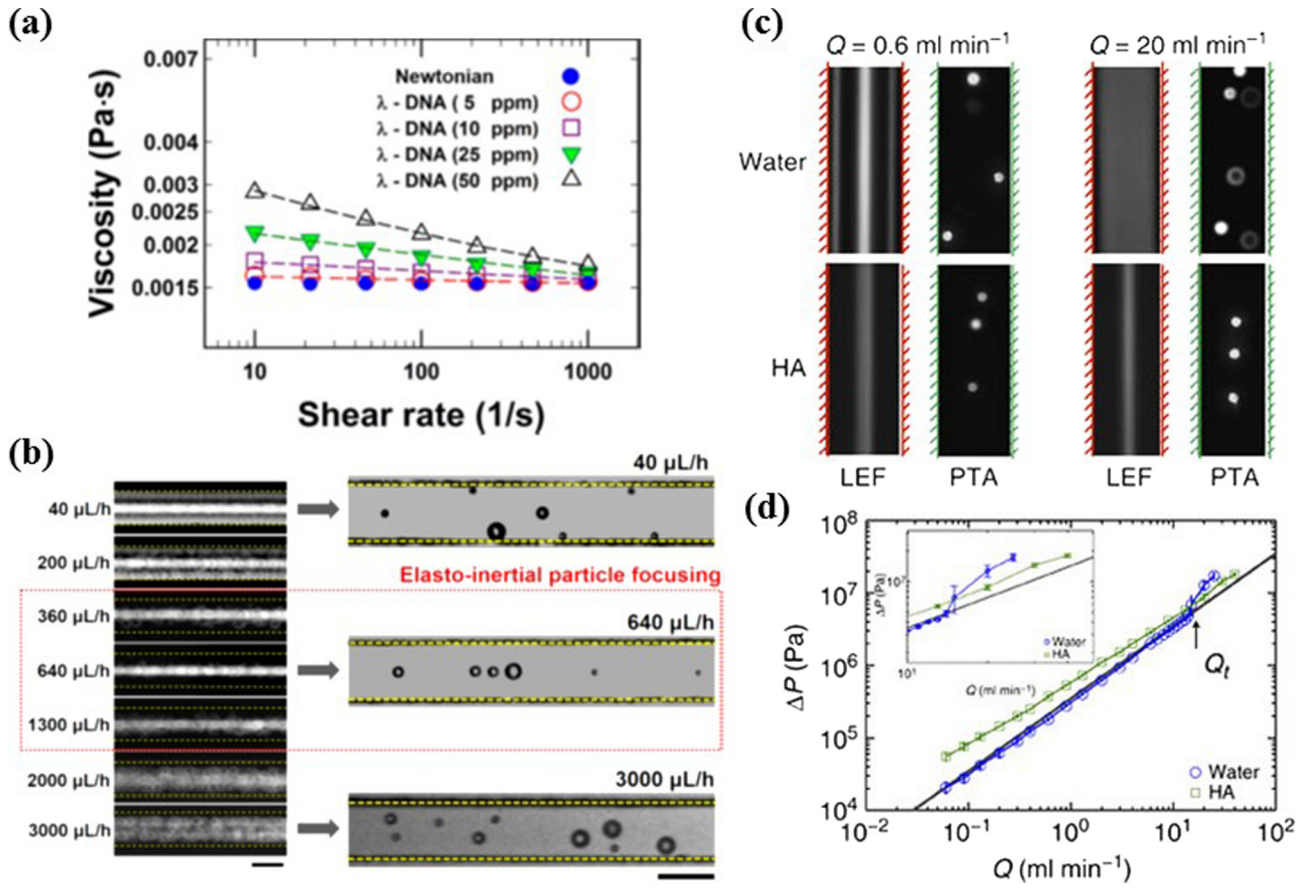

Fig. 5. Particle focusing in biofluid flows through straight square microchannels. (a) Viscosity vs. shear rate plot for λ-DNA solutions of different concentrations in 1× TE buffer with 13.8 wt.% sucrose. (b) Stacked (left column) and representative snapshot (right column) images illustrating the elasto-inertial focusing of 6 μm, 10 μm and 15 μm diameter particle mixture in the flow of 5 ppm λ-DNA solution through a 50 μm wide square channel. Adapted with permission from Kim and Kim [108], © 2016 AIP Publishing LLC. (c) Fluorescent images of 8 μm diameter particles in water (top row) and HA solution (bottom row) at the flow rates of 0.6 ml/min and 20.0 ml/min (corresponding to $Re = 4630$ in water and $Re = 4422$ and $Wi = 566$ in HA with $El = 0.13$), respectively. (d) Measured pressure drops across the fluidic system filled water and HA solution, respectively. The inset plot shows pressure drops near the onset of inertially turbulent water flow at the flow rate, $Q_t \approx 12$ ml/min. Adapted with permission from Lim et al. [29], © 2014 Macmillan Publishers Limited.

observed deterministic particle migration in 0.1% HA solution (1650 kDa molecular weight) toward the centerline of an 80 μm wide square microchannel over a wide range of flow rates with $10 \leqslant Re \leqslant 10,000$ (Fig. 5c). This inertio-elastic particle focusing at *Re* well beyond the upper limit for inertial focusing in a Newtonian fluid [21–25] is attributed to the viscoelastic tension along fluid streamlines (due to the first normal stress difference) that stabilizes the flow and delay its transition to turbulence (Fig. 5d).

3.2.3. Rectangular microchannels

Elasto-inertial particle focusing becomes more interesting in rectangular microchannels with an intermediate aspect ratio, $AR = width/height$, than in slit-like and square ones. This is because the elastic lift, $\mathbf{F}_{eL}$ in Eq. (9), and inertial lift, $\mathbf{F}_{iL}$ in Eq. (7), are both a strong function of fluid shear rate that varies significantly with *AR* in the channel cross section. The competition of these two lateral forces [109] (Fig. 6a) has been demonstrated to result in fluid and particle properties dependent equilibrium positions in straight rectangular microchannels. Liu et al. [110] observed in a straight rectangular microchannel with $AR = 2$ differential elasto-inertial focusing of 5 μm and 15 μm diameter particles in 2000 ppm PEO solution (Fig. 6b). In a certain range of flow rates the larger particles are focused to two equilibrium off-center positions that are symmetric about the single equilibrium position of the smaller particles along the channel centerline. Moreover, the focusing positions of both types of particles exhibit a shifting from multiple (centerline and corners) to one (centerline) and then to two with the increase of flow rate. Xiang et al. [111] later reported in a rectangular microchannel with $AR = 3$ multi-train elasto-inertial focusing of 10 μm diameter particles in 500 ppm PEO solution at three different positions of the vertical plane (Fig. 6c). They proposed a four-stage mechanism to explain the observed shifting of equilibrium particle positions with the increase in flow rate (Fig. 6d), which is, however, unable to fully explain the experimental observations in a rectangular microchannel with $AR = 2$ (Fig. 6e). In another study Kim et al. [26] demonstrated a weak centerline focusing of DNA molecules in 500 ppm PEO solution in a 30 μm wide, 10 μm high rectangular microchannel.

3.3. Rectangular microchannels with curved streamlines

3.3.1. Spiral microchannels

Lee et al. [112] introduced a multiplex particle focusing phenomenon in a viscoelastic fluid flow through a spiral microchannel that arises from the hydrodynamic interaction between the viscoelastic lift and the Dean drag (Fig. 7a). They observed single-line focusing of PS particles with a range of diameters at the outlet of a rectangular 10-loop single-spiral microchannel in dilute PEO solutions (Fig. 7b). Moreover, the larger particles were found to move closer to the outer wall than the smaller particles due to the dissimilar size-dependences of elastic lift (inertial lift was assumed small) and Dean drag. Xiang et al. later [113] performed

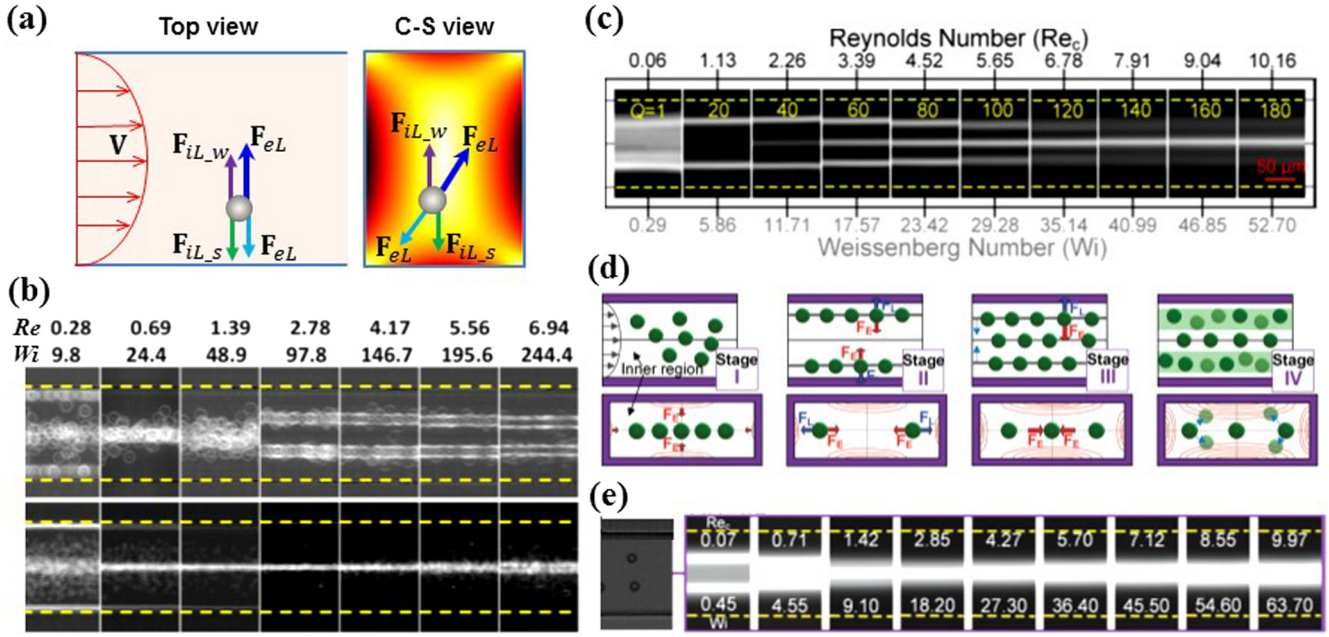

Fig. 6. Elasto-inertial particle focusing in straight rectangular microchannels with $AR \neq 1$ (i.e., not square) and $AR \neq 0$ (i.e., not slit-like). (a) Schematic for the forces exerted on a neutrally buoyant particle in a viscoelastic fluid flow through a straight rectangular microchannel. Adapted with permission from Li et al. [109], © 2016 American Chemical Society. (b) Stacked top-view images for the elasto-inertial focusing of 15 μm (top row) and 5 μm (bottom row) diameter PS particles in the flow of a denaturized 2000 ppm PEO solution through a 100 μm wide and 50 μm height (i.e., $AR = 2$) straight rectangular microchannel. Adapted with permission from Liu et al. [110], © 2015 American Chemical Society. (c) Stacked top-view images for the elasto-inertial focusing of 10 μm diameter particles in 500 ppm PEO solution in a 150 μm wide and 50 μm height (i.e., $AR = 3$) straight rectangular microchannel. (d) Schematic for the mechanism of elasto-inertial particle focusing in a straight rectangular microchannel. (e) Stacked top-view images of 10 μm diameter particles in 500 ppm PEO solution in a 100 μm wide and 50 μm height (i.e., $AR = 2$) straight rectangular microchannel. Adapted with permission from Xiang et al. [111], © 2016 AIP Publishing LLC.

a systematic study of elasto-inertial particle focusing in rectangular single-spiral microchannels over a wide range of flow rates, channel aspect ratios and channel radii. They found that with the increase of flow rate, particles undergo a dynamic process developing from dispersion to single-line focusing and finally multiple-streak defocusing (Fig. 7c). They also proposed a six-stage process model to explain the observed particle focusing process in Dean-coupled elasto-inertial flows. In a recent study Liu et al. [28] demonstrated a high-quality focusing of various nanoparticles in PEO solutions of low molecular weight that can offer sufficient elastic forces while at minimized shear thinning effects. They achieved an over 80% focusing efficiency for both 100 nm diameter PS particles (Fig. 7d) and λ-DNA molecules in the flow of PEO solution with a molecular weight of 0.6 MDa through a double-spiral microchannel. They observed a decreasing focusing efficiency with the increase of PEO molecular weight (up to 4 MDa) [28].

3.3.2. Straight microchannels with side-wells

Cha et al. [114] demonstrated a single-stream particle focusing in an inertialess flow of 6.8% PVP solution along the centerline of a straight square microchannel that is inserted with an array of square wells along each sidewall (Fig. 8a). Under exactly identical experimental conditions, particles are instead focused to five equilibrium positions (i.e., at the centerline and four corners) if the side-wells are all removed (c.f., Fig. 4c). The authors attributed their observed 3D particle focusing phenomenon to the combined action of hoop stress and elastic lift, where the former, which arises from the curved fluid streamlines in the grooved regions, plays a similar role to the inertial lift in elasto-inertial focusing (c.f., Fig. 4a) by directing particles away from the corners (Fig. 8b). Yuan et al. [115] later studied the particle focusing phenomena in both Newtonian (DI water) and non-Newtonian (500 ppm PEO solution) fluid flows through a straight rectangular microchannel with repeated triangular wells along one sidewall only (Fig. 8c). They observed a single equilibrium particle position near the wall without side-wells in the PEO solution, which is distinctly different from that in DI water (Fig. 8d). These differences were explained through the hydrodynamic interactions between the flow-induced lift (inertial lift in DI water while inertial lift and elastic lift in PEO) and Dean drag forces due to the introduction of the side-wells.

3.4. Summary

Table 1 summarizes the various particle focusing phenomena in microchannel non-Newtonian fluid flows with the details of the important experimental conditions. The values of the dimensionless numbers, *Wi* and *Re*, for each work are also provided.

4. Particle separation

Particle separation refers to the division and sorting of particles into different sub-groups based on either extrinsic labels (e.g., fluorescent and magnetic tags) or intrinsic markers (e.g., particle morphology and electrical, mechanical properties etc.). It is critical to many biomedical, chemical and environmental applications such as diagnostics, therapeutics and cell biology [116]. A variety of microfluidic techniques, which rely on nearly every single force field that one can enumerate ranging from the ubiquitous gravity to acoustic, electric, hydrodynamic, magnetic and optical forces, have been developed to separate particles in a continuous flow of Newtonian fluids. The readers are suggested to refer to the recent review papers from, for example, Sajeesh and Sen [117], Shields et al. [118], Lee et al. [119], and Yan et al. [120]. This section reviews the particle separation approaches that have been demonstrated in microchannel non-Newtonian fluid flows.

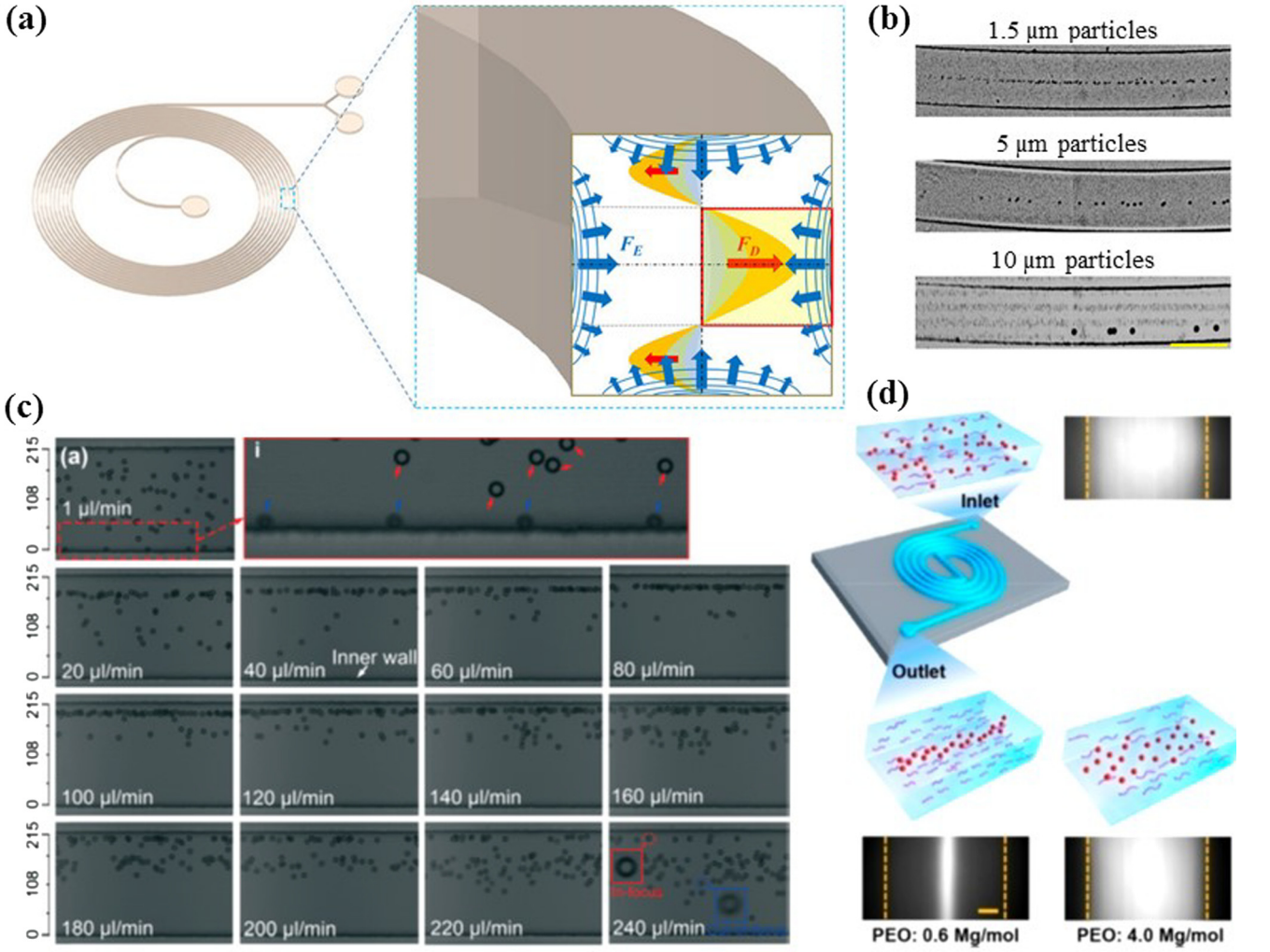

Fig. 7. Viscoelastic particle focusing in rectangular spiral microchannels. (a) Schematic diagram of the dean-coupled elasto-inertial focusing of particles in a single spiral microchannel [112]. (b) Experimental images illustrating the single-line focusing of particles with various diameters in PEO solution flow through a 100 μm wide and 25 μm high single-spiral microchannel [112]. (c) Stacked images showing the elasto-inertial focusing of 10 μm diameter particles in the flow 500 ppm PEO solution through a 215 μm wide and 50 μm high single-spiral microchannel. Adapted with permission from Xiang et al. [113], © 2016 The Royal Society of Chemistry. (d) Schematics and stacked fluorescent images for viscoelastic focusing of 100 nm diameter particles in the flow of PEO solutions (of different molecular weights) through a 30 μm wide and 4 μm high double spiral microchannel. Adapted with permission from Liu et al. [28], © 2016 American Chemical Society.

4.1. Sheath-flow separation by size

Nam et al. [121] demonstrated a high-purity separation of 1 μm and 5 μm diameter PS particles in 500 ppm PEO solution through a straight square microchannel (Fig. 9a). At the inlet trifurcation, the particle mixture in the suspension was focused toward the channel sidewalls by the central particle-free PEO sheath flow. The flow-induced elastic and inertial lift forces push the particles away from the sidewalls of the straight channel at a size-sensitive rate. As a result, the larger and smaller particles are sorted into the central and the two side branches, respectively, at the outlet trifurcation. The authors also applied their method to separate (smaller) platelets from dilute whole blood [121]. In spite of the variations in cell size, shape, and deformability, they still achieved a greater than 99.8% purity for the collected platelets. Lim et al. [64] later studied the effect of the second normal stress difference on this size-based sheath-flow particle separation in a similar structured rectangular microchannel (Fig. 9b, top row). They found that in both 100 ppm PAA and 500 ppm PEO solutions, the larger 10 μm diameter particles can reach the channel centerline at the outlet due to the action of the elasto-inertial lift. However, the smaller 1 μm diameter particles were observed to spread across the entire cross section in the PAA solution, which is different from the phenomenon in PEO due to the effect of the rotational secondary flow. This secondary flow effect is more influential on small particles, which is further confirmed by the displacement of small and large particles that are initially focused toward the channel centerline in the same microchannel (Fig. 9b, bottom row) [64].

In another study, Kang et al. [96] demonstrated a highly efficient separation of PS particles with four different diameters in the range of 1–10 μm in the flow of an extremely dilute λ-DNA solution (5 ppm) through a straight 4 cm long, 50 μm wide square microchannel (Fig. 9c). Due to its unique structural properties, DNA is an efficient elasticity enhancer that significantly promotes and segregates the lateral displacement of particles with subtle size differences for a high-resolution separation. As the microchannel in Fig. 9c has a similar structure to that used in pinched flow fractionation (PFF) [122], Lu and Xuan [123] termed this separation technique elasto-inertial pinched flow fractionation (eiPFF). They performed a comprehensive study of multiple parametric effects on eiPFF in terms of dimensionless numbers including *Re*, *Wi*, *El*, *AR* and the sheath to particle flow rate ratio (Fig. 9d). Interestingly,

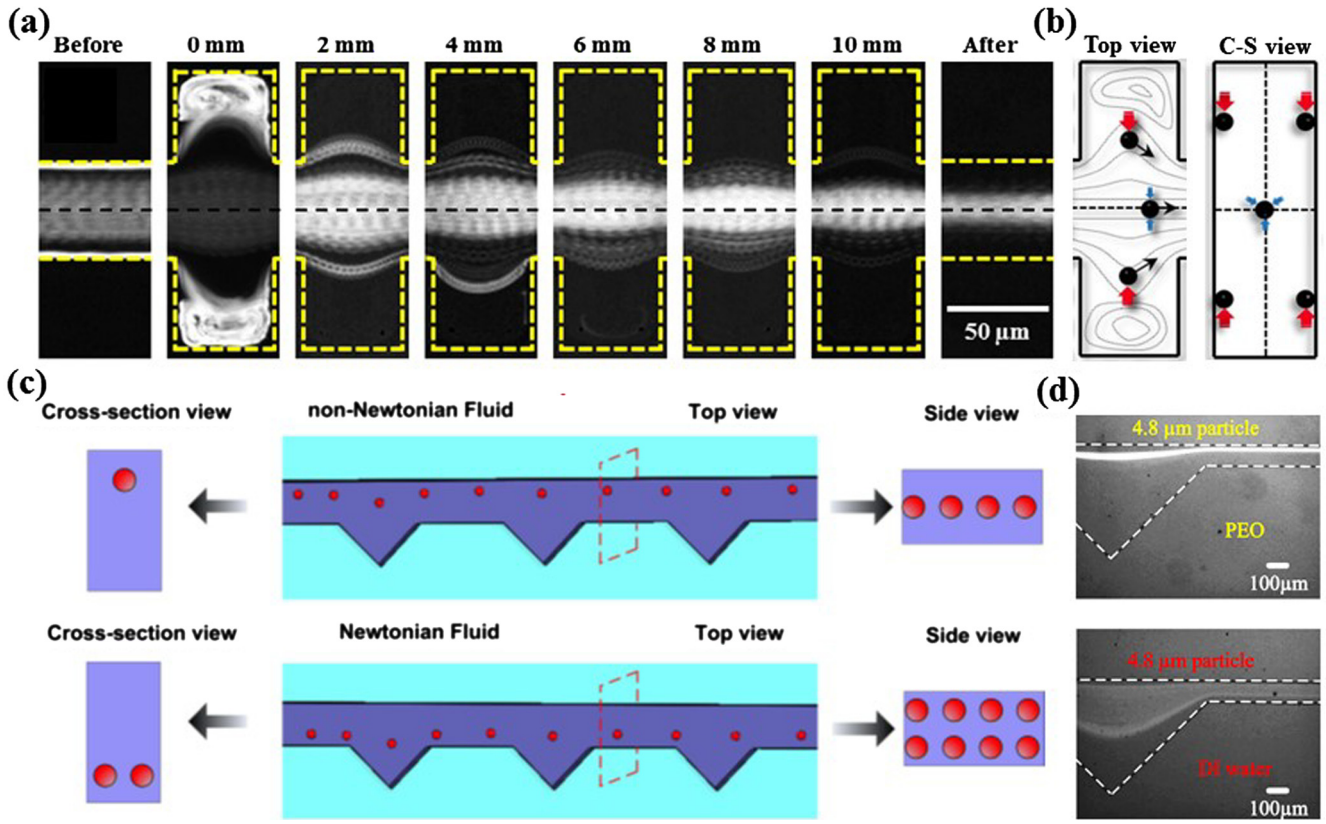

Fig. 8. Viscoelastic particle focusing in straight rectangular microchannels with side-wells. (a) Stacked images showing the centerline focusing of 6 μm diameter PS particles in the flow of 6.8% PVP solution through a 50 μm square microchannel with repeated square wells along both sidewalls at a flow rate of 300 μl/h. Adapted with permission from Cha et al. [114], © 2014 Springer. (b) Schematics showing the hoop stress (highlighted by the thickest red arrows)-assisted 3D elastic (highlighted by the thicker blue arrows) particle focusing in the top and cross-sectional views of the channel expansion, respectively [114]. (c) Schematic diagrams for the particle focusing phenomena in Newtonian and non-Newtonian fluid flows, respectively, through a straight rectangular microchannel with an array of triangular wells along one sidewall. Adapted with permission from Yuan et al. [115], © 2015 AIP Publishing LLC. (d) Top-view fluorescent images of 4.8 μm diameter particles in 500 ppm PEO solution (top row) and DI water (bottom row) at the outlet of a straight 100 μm wide and 40 μm deep microchannel with triangular side-wells under an identical flow rate of 60 μl/min [115]. (For interpretation of the references to colour in this figure legend, the reader is referred to the web version of this article.)

they found that the lateral displacement of 10 μm diameter particles from the (top) sidewall can be either smaller (at low flow rates) or larger (at high flow rates) than that of 3 μm particles in 1000 PEO solution in a rectangular microchannel with $AR = 2.0$ (i.e., 50 μm wide and 25 μm deep). This phenomenon was not observed in the 50 μm wide channels with both $AR = 0.5$ (i.e., 100 μm deep) and $AR = 1.25$ (i.e., 40 μm deep), and had not been reported in the literature either.

4.2. Sheath-free separation by size

The first attempt of sheath-free separation in non-Newtonian fluid flows was made by Yang et al. [30] in a single straight square microchannel. Due to the strong dependence of elastic and inertial lift forces on particle size, large particles in 250 ppm PEO solution become well focused along the channel centerline at the outlet expansion leaving out smaller particles largely dispersed (Fig. 10a). The result is a size-based enrichment of the large particles that can be collected along with part of the small particles into a central outlet [124]. A similar idea was later demonstrated by Yuan et al. [125] to extract plasma from diluted blood samples in PEO solutions via the 3D elasto-inertial focusing of blood cells in a straight rectangular microchannel with an array of triangular side-wells along one sidewall. In another study Nam et al. [126] proposed a two-stage microfluidic device for sheath-free particle separation in a viscoelastic fluid flow (Fig. 10b). Particles are elasto-inertially focused to the centerline of a circular microchannel at the 1st stage and subsequently deflected by the elastic lift to size-dependent flow paths in two symmetrically arranged rectangular microchannels at the 2nd stage. The device was first tested with the separation of 5 μm and 10 μm diameter PS particles in a highly elastic 8% PVP solution at very low flow rates with $Re < 0.01$ [126]. It was later improved for the separation of tumor cells from leukocytes in a weakly elastic 0.1% HA solution at a throughput of 4×10^5 cells/min (200 μl/min) [127]. Recently the authors have further revised their device by replacing the circular microchannel at the 1st stage with a slit-like microchannel and optimizing the dimensions of the rectangular microchannel at the 2nd stage. The new device was demonstrated to separate malaria parasites from a lysed blood in 0.1% HA solution at a flow rate of 400 μl/min with over 90% recovery rate and purity [128].

Sheath-free particle separation in viscoelastic fluid flows has also been implemented in single straight rectangular microchannels. Liu et al. [110] utilized the differential elasto-inertial focusing to separate PS particles by size in 2000 ppm PEO solution flows through rectangular microchannels with a high AR. They further applied their technique to separate MCF-7 cancer cells from RBCs in a 100 μm wide/50 μm high microchannel (i.e., $AR = 2.0$), and RBCs from *Escherichia coli* (*E. coli*) in a 40 μm wide/10 μm high microchannel (i.e., $AR = 4.0$) (Fig. 10c, top row). In both experiments, the larger and smaller cells were observed to migrate to two off-center equilibrium positions and one centerline equilibrium position (Fig. 10c, bottom row), respectively, which is consistent with the focusing phenomena of similar sized PS particles

Table 1
Summary of particle focusing phenomena in microchannel non-Newtonian fluid flows.

Ref.	Channel structure	Channel dimension	Fluid	Particle (d in μm)	Particle flow rate	Wi[a]	Re[a]
Santo et al. [27]	Straight cylindrical	5 μm dia.	3000 ppm PEO	PS (0.2)	16.2 nl/h	0.12	1.5e−4
Seo et al. [85]	Straight cylindrical	300 μm dia.	8% PVP	PS (7, 15, 30)	1.2–30 ml/h	0.2–5	0.03–0.74
D'Avino et al. [93]	Straight cylindrical	50 μm dia.	8% PVP 1% PEO	PS (4)	0.45–45 μl/h	0.005–0.2	≤1e−3
Kang et al. [96]	Straight cylindrical	50 μm dia.	5 ppm λ-DNA	PS (5.8, 10.5)	5–2000 μl/h	4–1600	0.018–7.2
Romeo et al. [99]	Straight cylindrical	50 μm dia.	8% PVP	PS (2.4, 5.9)	0.6–6 μl/h	0.005–0.05	≤5e−4
Leshansky et al. [88]	Straight slit-like	1000 × 45 μm^2	8% PVP 45 ppm PAA	PS (5, 8)	0.4–2 ml/h	0.0056–0.028 0.025–0.12	0.0033–0.017 0.0041–0.02
Seo et al. [102]	Straight slit-like	500 × 50 μm^2 300 × 30 μm^2	8%, 3% PVP	PS (7.22) RBCs	0.06–3 ml/h	0.53–27	0.001–0.06
Yang et al. [30]	Straight square	50 × 50 μm^2	500 ppm PEO	PS (5.9)	0.20 ml/h	8.04	0.37
Del Giudice et al. [105]	Straight square	50 × 50 μm^2 100 × 100 μm^2	8% PVP	PS (5.8, 10)	1.6–530 μl/h	0.0045–0.2	9.5e−5 to 0.016
Seo et al. [86]	Straight square	300 × 300 μm^2	8% PVP 1% PEO	PS (30, 50)	1.2–60 ml/h	4.9–247 1.2–60	0.02–1.11 0.01–5.56
Del Giudice et al. [106]	Straight square	100 × 100 μm^2	0.1, 0.8, 1.6% PEO	PS (10)	0.073–2.67 ml/h	0.033–9.2	6.7e−5 to 0.3
Song et al. [107]	Straight square	50 × 50 μm^2	0.01–1% PEO	PS (4.78)	40–320 μl/h	0.26–25.6	0.004–0.8
Kim et al. [26]	Straight square	5 × 5 μm^2	500 ppm PEO	PS (0.1, 0.2, 0.5, 1, 2.4)	5–15 μl/h	178–533	0.11–0.33
Kim and Kim [108]	Straight square	50 × 50 μm^2	2.5–50 ppm λ-DNA	PS (10)	0.04–3 ml/h	20–1491	0.14–10.6
Lim et al. [29]	Straight square	80 × 80 μm^2	0.1% HA	PS (8)	5.4–1200 ml/h	2.6–566	11–4422
Liu et al. [110]	Straight rectangular	200 × 50 μm^2 100 × 50 μm^2 50 × 50 μm^2	2000 ppm PEO	PS (5, 15)	0.2–10 ml/h	6.1–244.4	0.28–13.89
Xiang et al. [111]	Straight rectangular	150 × 50 μm^2 100 × 50 μm^2 50 × 50 μm^2	500 ppm PEO 8% PVP	PS (2, 5, 10)	1–180 μl/min	0.07–97.07	0.001–10.16
Lee et al. [112]	Spiral rectangular	100 × 20 μm^2	500–5000 ppm PEO	PS (1.5, 5, 10)	50–750 μl/h	0.03–13.4	0.1–1
Xiang et al. [113]	Spiral rectangular	215 × 50 μm^2 140 × 50 μm^2 90 × 50 μm^2	500 ppm PEO	PS (5, 10)	1–240 μl/min	0.17–41.8	0.04–9.66
Liu et al. [28]	Spiral rectangular	30 × 4 μm^2	0.2–2% PEO in Tris-EDTA	PS (0.1, 0.049) DNA	0.32–2.45 μl/h	0.09–0.67	<0.005
Cha et al. [114]	Square side-wells	50 × 50 μm^2	6.8% PVP	PS (6)	0.12–1 ml/h	0.68–5.7	0.012–0.1
Yuan et al. [115]	Triangular side-walls	100 × 40 μm^2	500 ppm PEO	PS (3.2, 4.8, 13)	1.8–7.2 ml/h	22.74–90.96	2.31–9.24

[a] Note: estimated based on the giving fluid properties if not provided in the paper.

[110]. Later, Li et al. [109] presented a systematic experimental study of multiple parametric effects on a binary separation of 5 μm and 10 μm diameter PS particles in viscoelastic fluid flows through straight rectangular microchannels. They proposed to break down the elastic lift, analogous to that of the inertial lift into the wall- and shear gradient-induced components [21–25], into a center-directed and a wall-directed component due to fluid elasticity and/or shear thinning effects for understanding the observed shifting of particle focusing positions. They also demonstrated a sheath-free separation of 3 μm, 5 μm and 10 μm diameter particles in 1000 ppm PEO solution in a 50 μm wide and 25 μm high microchannel (Fig. 10d). Recently Liu et al. [28] has demonstrated a viscoelastic separation of 100 nm/2 μm PS particles and λ-DNA molecules/platelets in 0.6 wt.% low-molecular-weight PEO solution through a 30 μm wide/4 μm high double spiral microchannel. The flow-induced elastic lift and Dean drag acts together to focus the nanoparticles and microparticles toward the channel center and sidewalls, respectively. A similar idea was also demonstrated earlier by Lee et al. [112] to separate 1.5 μm and 10 μm diameter PS particles in the flow of PEO solution through a single spiral microchannel.

4.3. Separation based on other intrinsic markers

There have been a few attempts in the literature to separate particles in viscoelastic fluid flows based on the difference in particle shape or deformability. Lu and Xuan [129] applied the technique, eiPFF, which had been demonstrated effective for size-based particle separation [123], to separate spherical and peanut-shaped PS particles of nearly equal volume with a sheath-flow pre-focusing (Fig. 11a, top row). They observed a larger deflection of 5 μm spheres from the wall than that of 3.5 μm diameter/6 μm length peanuts in 1000 ppm PEO solution in a straight rectangular microchannel of 50 μm width and 25 μm height [129] (Fig. 11a, bottom row). This phenomenon indicates the strong shape-dependence of the flow-induced elasto-inertial lift, which, through a high-speed imaging of particle motion, is speculated to correlate with the rotational effects of non-spherical particles. Lu et al. [130] later found that the differential elasto-inertial focusing, which had been demonstrated to separate particles by size in a sheath-free manner [110], is also capable of separating the spherical and peanut particles in 1000 ppm PEO solution flow at greater than 95% efficiency and purity (Fig. 11b). It is because the two types of particles transit from single centerline equilibrium position to dual off-center equilibrium positions at different flow rates. This sheathless shape-based particle separation is, however, strongly affected by the flow rate (Re), PEO concentration (Wi) and channel depth (AR). Yang et al. [131] observed in an inertialess flow of PBS-based 6.8 wt.% PVP solution an inward migration of deformable RBCs toward the centerline of a straight 50 μm wide square microchannel. This is different from the center- and corner-directed migrations of rigid PS particles due to the dominant cell deformability-induced lift over the elastic lift near the channel corners (Fig. 11c, left). The authors used these phenomena to separate PS particles from RBCs (Fig. 11c, right), and as well less deformable white blood cells (WBCs) from diluted whole blood with a high enrichment ratio.

4.4. Viscoelastic focusing-based magnetic separation

The flow-induced elasto-inertial effect in viscoelastic fluids has been utilized to pre-focus particles for a continuous sheath-free

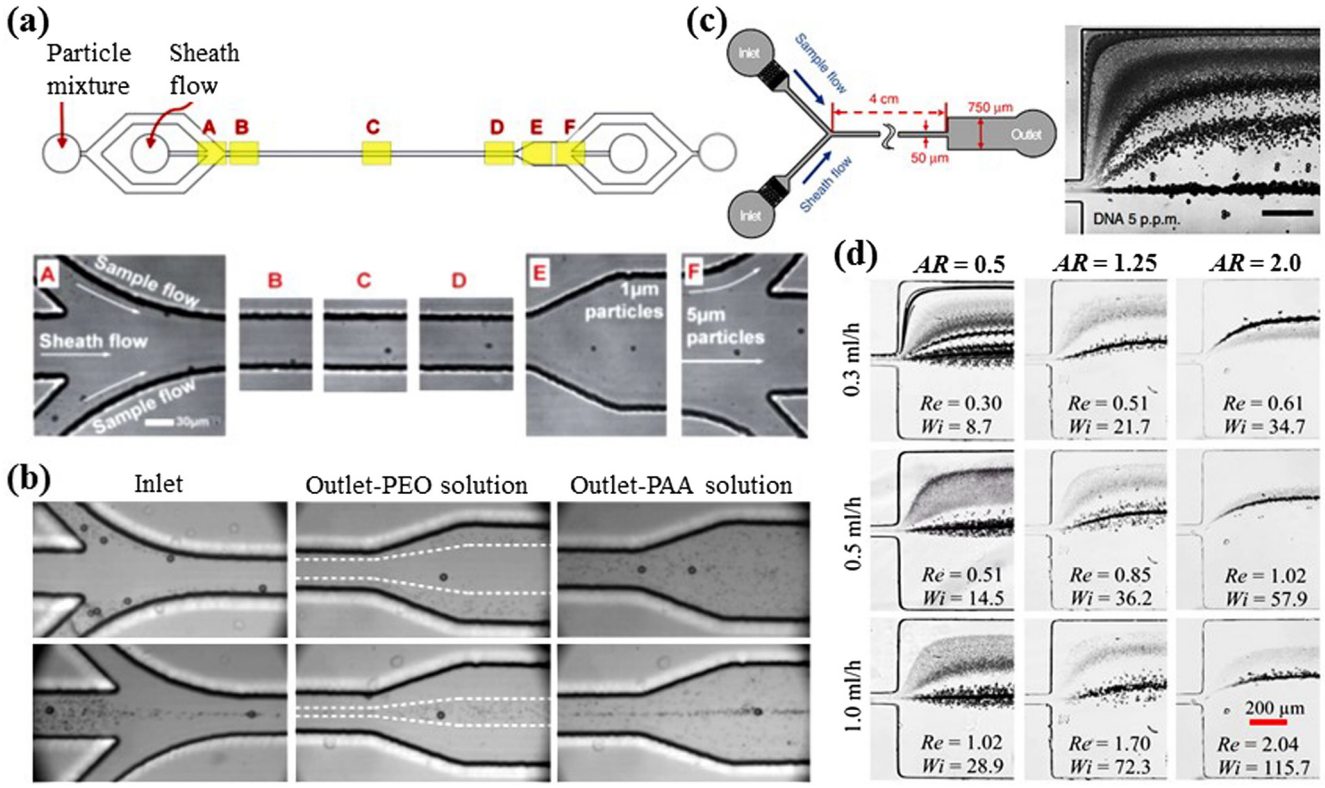

Fig. 9. Sheath-flow separation of particles by size in viscoelastic fluid flows. (a) Snapshot images illustrating the lateral displacement of sheath flow-focused 1 μm and 5 μm diameter particles in 500 ppm PEO solution at different axial locations of a straight 2.5 cm long, 50 μm wide square microchannel. Adapted with permission from Nam et al. [121], © 2012 The Royal Society of Chemistry. (b) Snapshot images comparing the lateral displacement of 1 μm and 10 μm diameter particles in 500 ppm PEO (middle column) and 100 ppm PAA (right column) solutions when the particle mixture is initially focused toward the sidewalls (top row) and centerline (bottom row) of a straight 100 μm wide, 50 μm deep microchannel. Adapted with permission from Lim et al. [64], © 2014 Springer. (c) Schematic illustration of the microchannel and stacked image at the channel expansion demonstrating the separation of 1 μm, 2.3 μm, 4.5 μm and 10.5 μm diameter PS particles in 5 ppm λ-DNA solution. Adapted with permission from Kang et al. [96], © 2013 Macmillan Publishers Limited. (d) Stacked images illustrating the effect of channel aspect ratio (*AR*) on the separation of 3 μm and 10 μm diameter particles in 1000 ppm PEO solution via eiPFF in 100 μm, 40 μm and 25 μm (from left to right) deep microchannels, respectively, with a fixed 50 μm width. Adapted with permission from Lu and Xuan [123], © 2015 American Chemical Society.

magnetic separation. Del Giudice et al. [132] first demonstrated such a hybrid separation in an H-shaped microchannel (Fig. 12a, top), where the buffer in the top branch is a particle-free solution for collecting the sorted magnetic particles. 10 μm magnetic and 20 μm diamagnetic particles are elastically focused in an inertialess flow of 0.5 wt.% polyacrylamide (PAM) solution through a 100 μm wide and 50 μm high microchannel prior to be separated at the outlet bifurcation by the use of a permanent (Fig. 12a, bottom). The authors found that the pre-focusing enhances the deflection/separation efficiency of magnetic particles and also has a positive effect in contrasting their sedimentation. Kim et al. [133] reported a two-step separation of diamagnetic particles by size using elasto-inertial focusing and magnetophoresis in a mixed PEO (0.4 wt.%) and ferrofluid (0.1 × EMG 408) medium (Fig. 12b). In the first step, the PEO flow-induced elasto-inertial force focuses particles into a single stream along the centerline of a straight 50 μm wide square microchannel. In the second step, the ferrofluid-induced magnetic force deflects the particles away from the magnet toward size-dependent flow paths in a 250 μm wide rectangular chamber (Fig. 12b). The authors also tested their device with two different-sized biological cells, *Chlorella vulgaris* and *Synechococcus* sp., and investigated the viability of cells after the separation [133]. A similar two-stage microfluidic sorter was later developed by Zhang et al. (Fig. 12c), who demonstrated the benefit of using PEO-based ferrofluid by comparing the separation of 5 μm and 13 μm diameter diamagnetic particles therein with that in a conventional aqueous ferrofluid [134].

4.5. Summary

Table 2 summarizes the above-reviewed various particle separation methods in non-Newtonian microfluidic devices with the details of the important experimental conditions. The values of the related dimensionless numbers are also provided.

5. Other particle manipulations

5.1. Particle medium exchange

Particle medium exchange refers to the transfer of particles from one suspending medium to the other for their washing, coating or any other purposes [135]. As reviewed above, viscoelastic polymer solutions have been widely used to focus and separate PS particles of various sizes, shapes and properties (e.g., magnetization). Their applications to cells or other bioparticles are, however, still very limited due to the concern of biocompatibility [23,24]. It is therefore desirable to transfer particles out of the non-Newtonian fluid stream, if at all possible, after the necessary manipulation therein (e.g., focusing and separation). Ha et al. [136] engineered the flow-induced elastic and inertial lift forces to transfer particles across a non-Newtonian stream and into a Newtonian stream (Fig. 13a, top row). Such a cross-stream particle migration is due to the action of the elastic lift in the non-Newtonian fluid side and the inertial lift in the Newtonian fluid

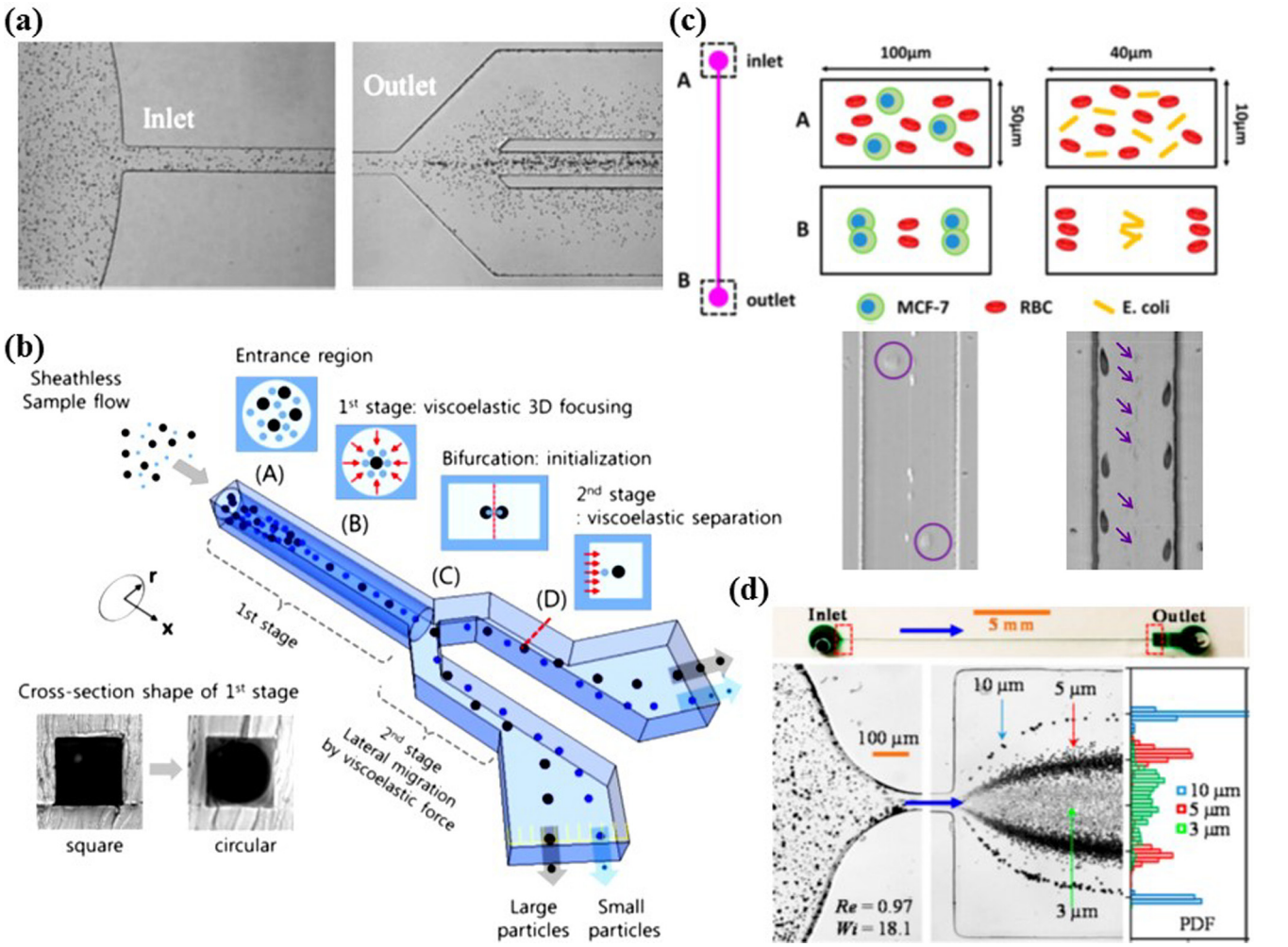

Fig. 10. Sheath-free separation of particles by size in microchannel viscoelastic fluid flows. (a) Snapshot images showing the size-based enrichment of 4.5 μm diameter PS particles from 2.3 μm ones in the flow of 250 ppm PEO solution through a straight 4 cm long, 50 μm wide square microchannel. Adapted with permission from Ahn et al. [124], © 2014 Elsevier Ltd. (b) Schematic illustration of a two-stage microfluidic device for sheathless focusing and size-based separation of particles in viscoelastic fluid flows. Adapted with permission from Nam et al. [126], © 2015 Elsevier Ltd. (c) Schematic (top row) and snapshot images (bottom row) of size-based cell separation in PEO solution flows through straight rectangular microchannels. Adapted with permission from Liu et al. [110], © 2015 American Chemical Society. (d) Images at the inlet/outlet and probability distribution function (PDF) at the outlet expansion for a ternary particle separation in 1000 ppm PEO solution through a straight 50 μm wide and 25 μm high rectangular microchannel. Adapted with permission from Li et al. [109], © 2016 American Chemical Society.

side, which together leads to a single stable equilibrium position within the Newtonian fluid stream (Fig. 13a, bottom row). The authors used their device to demonstrate a simultaneous washing and separation of 9.9 μm diameter PS particles from 2.0 μm ones that are left behind within a dilute λ-DNA solution due to their slower elastic migration (Fig. 13b). In another independent study, Yuan et al. [137] observed a lateral migration of 4.8 μm diameter PS particles from 1000 ppm PEO solution into DI water in an inertialess flow through a straight 30 μm wide and 50 μm high rectangular microchannel (Fig. 13c). They also studied the effects of channel length, flow rate and PEO concentration on such a cross-stream transfer of particles.

5.2. Particle stretching

Particle stretching refers to the deformation of particles under a stress field, which has been often used to monitor and measure the mechanical properties of cells that are associated with, for example, their disease state [138]. Cha et al. [139] developed an efficient method to measure cell stretching in a cross-slot microchannel by the use of 3D viscoelastic focusing (Fig. 14a). The flow-induced elastic lift in a biocompatible (PBS-based 6.8% PVP solution) viscoelastic suspending medium aligns cells along the centerline of each 50 μm wide square input branch of the cross-slot. As such, the majority of the focused cells can be delivered to the stagnation point of the cross-slot and stretched by the extensional flow that is formed by the symmetric fluid flows from/to the two input/output branches, respectively. Moreover, this cell stretching is free of rotation because the stagnation point is along the shear-free centerline of the microchannel. This method has been demonstrated to stretch RBCs [139] and Chinese hamster ovary (CHO) cells [140] (Fig. 14b). In another interesting work, Lim et al. [29] reported a simultaneous focusing and stretching of WBCs in weakly elastic HA solutions along the centerline of a single straight square microchannel at high throughput. This phenomenon results from the combined actions of the flow-induced elastic lift (for cell focusing) and the normal stress difference-induced additional tensile stress along fluid streamlines (for cell stretching). Moreover, the rheological properties of the HA solution can be tuned to generate an optimal balance between cell focusing and stretching over a wide range of Reynolds numbers (Fig. 14c).

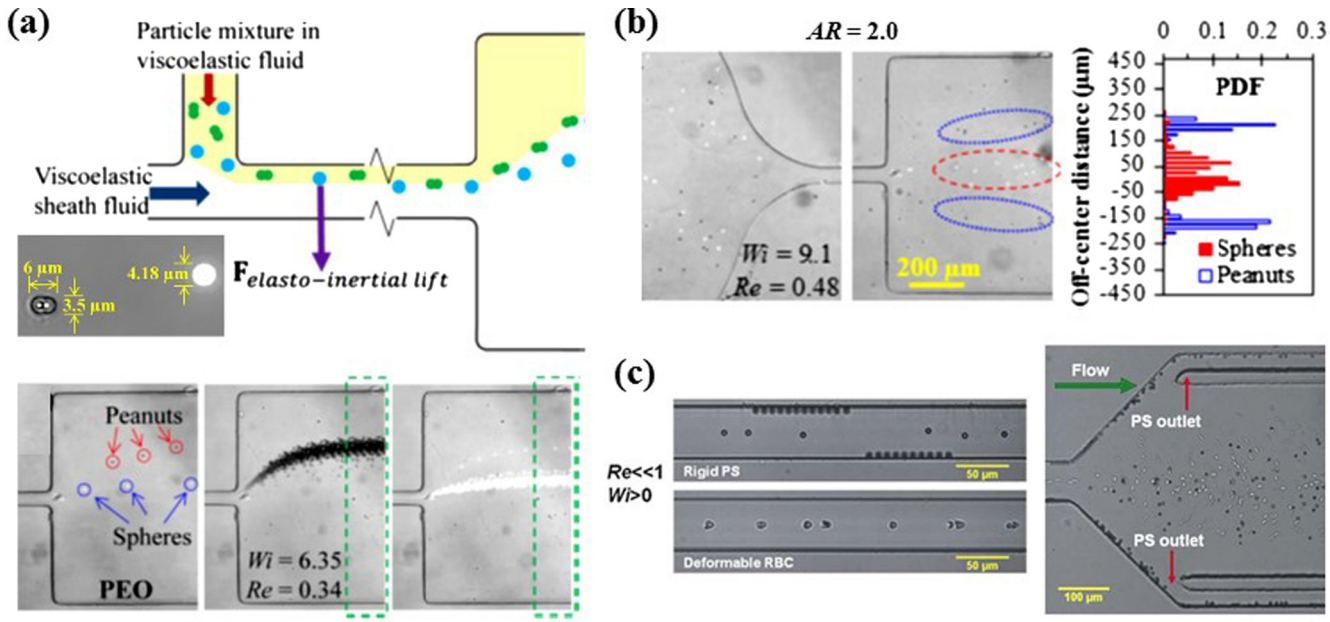

Fig. 11. Viscoelastic separation of particles by intrinsic non-size markers. (a) Schematic illustration (top row) and experimental images (bottom row) for sheath-flow separation of peanut and spherical PS particles of equal volume (inset image) via eiPFF in 1000 ppm PEO solution through a straight 50 μm wide/25 μm high rectangular microchannel. Adapted with permission from Lu and Xuan [129], © 2015 American Chemical Society. (b) Snapshot images at the inlet/outlet and probability distribution function (PDF) at the outlet expansion for sheathless separation of peanut and spherical particles in 1000 ppm PEO solution in a single straight 50 μm wide/25 μm high rectangular microchannel. Adapted with permission from Lu et al. [130], © 2015 AIP Publishing LLC. (c) Snapshot images for the elastic focusing (left) of rigid 6 μm diameter PS particles and their elastic separation (right) from deformable RBCs (stained in the right image) in 6.8 wt.% PVP solution flows through straight square microchannels under negligible inertia. Adapted with permission from Yang et al. [131], © 2012 The Royal Society of Chemistry.

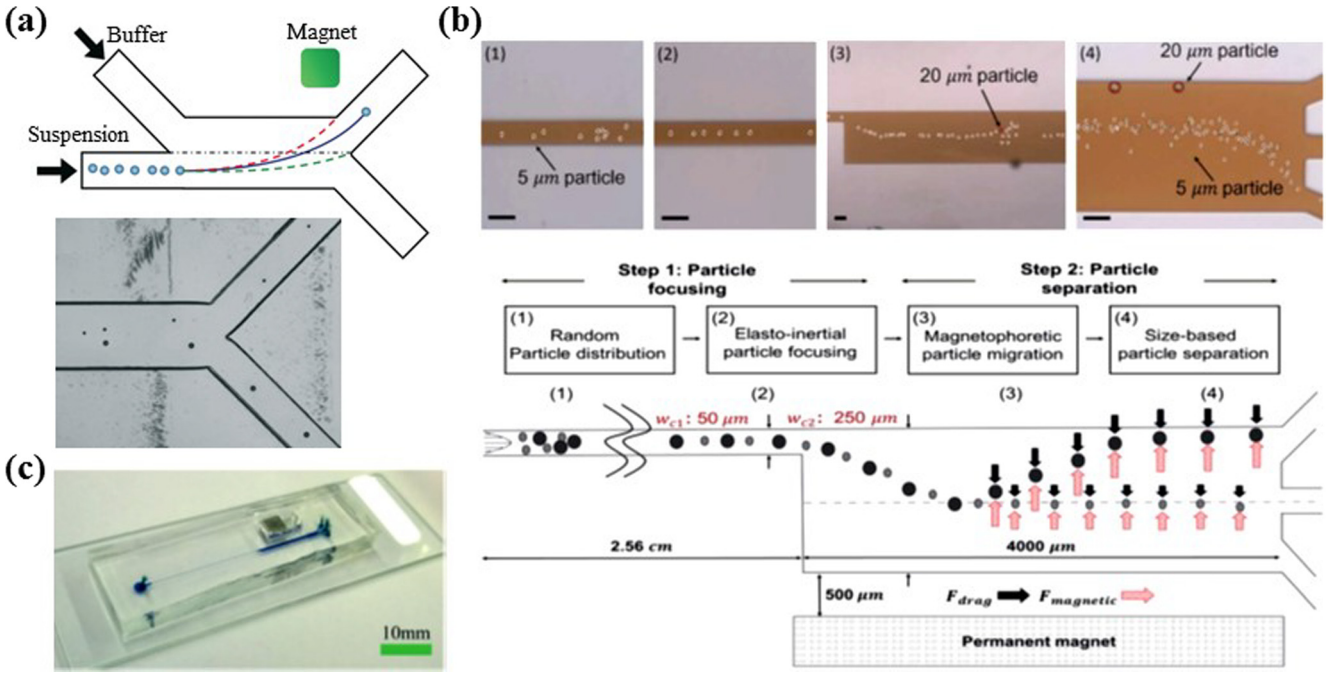

Fig. 12. Viscoelastic focusing-based magnetic separation of particles. (a) Schematic diagram (top) and snapshot image at the outlet bifurcation (bottom) for the magnetic separation of elastically pre-focused 10 μm magnetic and 20 μm diamagnetic particles in 0.5 wt.% polyacrylamide (PAM) solution. Adapted with permission from Del Giudice et al. [132], © 2015 The Royal Society of Chemistry. (b) Experimental images at different locations (top row) and schematic view (bottom row) of a two-step separation of diamagnetic particles by size in a dilute PEO/ferrofluid medium. Adapted with permission from Kim et al. [133], © 2016 The Royal Society of Chemistry. (c) Picture of a two-stage microfluidic device for continuous sheathless separation of diamagnetic particles in a viscoelastic PEO-based ferrofluid. Adapted with permission from Zhang et al. [134], © 2016 The Royal Society of Chemistry.

5.3. Summary

Table 3 summarizes the recent demonstrations of particle washing and stretching in non-Newtonian microfluidic devices with the details of the important experimental conditions.

6. Conclusions and perspectives

The diverse particle manipulations, including focusing, separation, washing and stretching, in non-Newtonian microfluidic devices have been reviewed in this article. As viewed from the

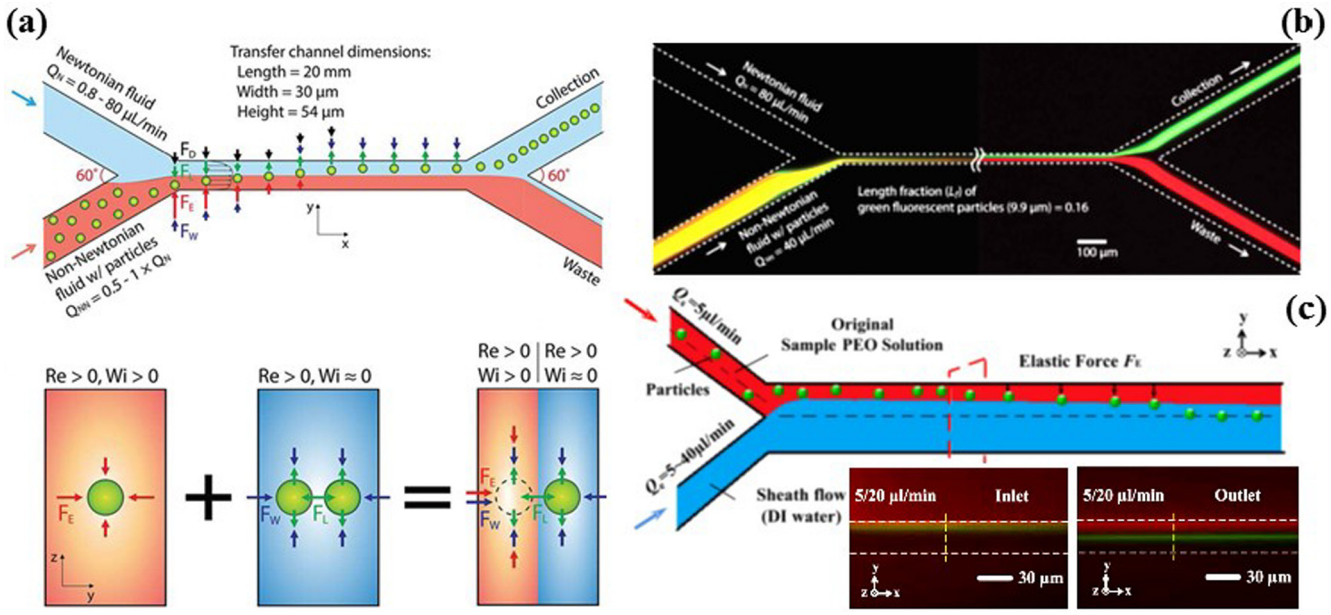

Fig. 13. Particle medium exchange from non-Newtonian to Newtonian. (a) Schematic of particle migration across a non-Newtonian fluid stream and into a Newtonian fluid stream (top row) due to the single stable equilibrium particle position inside the Newtonian fluid (bottom row). (b) Stacked fluorescent images illustrating the simultaneous washing and separation of 9.9 μm diameter particles (green) from 2.0 μm diameter particles (red) that remain suspended in 0.01% (w/v) λ-DNA solution. Adapted with permission from Ha et al. [136], © 2016 American Chemical Society. (c) Schematic diagram and experimental images (inset) of particle lateral migration from 1000 ppm PEO solution into DI water in a straight rectangular microchannel. Adapted with permission from Yuan et al. [137], © 2016 WILEY-VCH Verlag GmbH & Co.

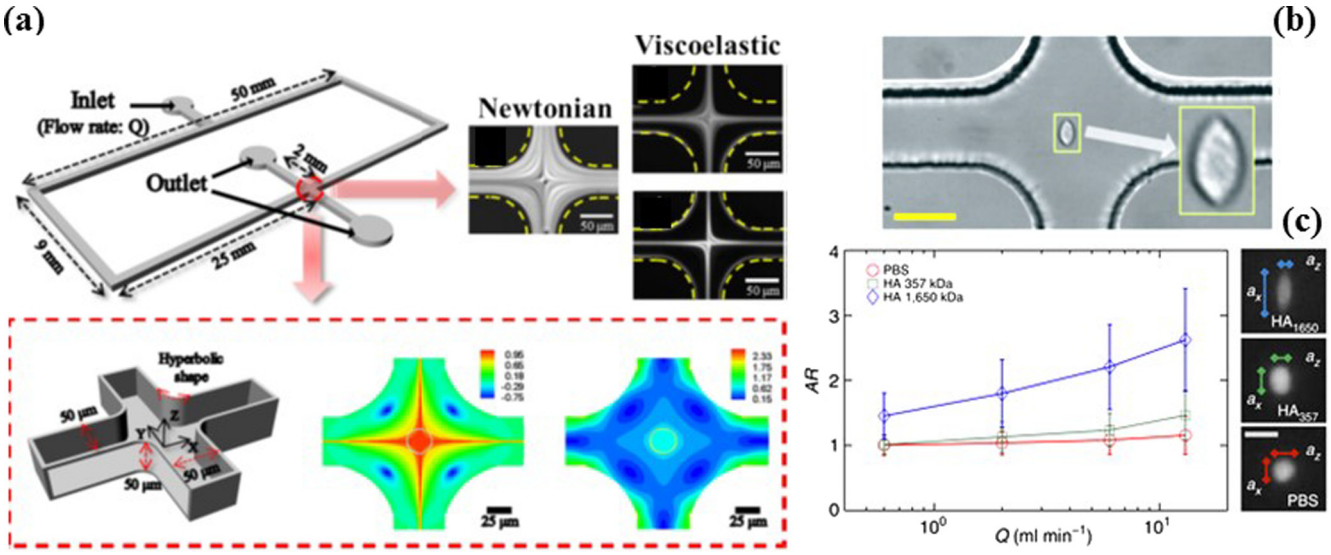

Fig. 14. Particle stretching in microchannel non-Newtonian fluid flows. (a) Schematic of the microfluidic device where the insets at the bottom show the magnified view of the cross-slot geometry and flow simulations, and those at the right show the trajectories of PS particles in Newtonian and viscoelastic media. Adapted with permission from Cha et al. [139], © 2012 American Chemical Society. (b) Sample image of a stretched CHO cell at the stagnation point of the cross-slot geometry in (a). Adapted with permission from Bae et al. [140], © 2016 The Royal Society of Chemistry. (c) Comparison of WBC deformations (in terms of cell aspect ratio) in the flows of PBS and low/high molecular-weight HA solutions through a single straight 80 μm wide square microchannel. Adapted with permission from Lim et al. [29], © 2014 Macmillan Publishers Limited.

dimensionless numbers summarized in Tables 1–3, the majority of these operations are demonstrated only in low *Re* (on the order of 1 or less) flows where the inertial effect is either negligible or still weak as compared to the elastic effect. Interestingly, they all take place in particle suspensions based on synthetic polymers (i.e., PEO and PVP, etc.), where the value of *Wi* is usually at least one order of magnitude greater than that of *Re* (or in other words, the elasticity number, *El*, is on the order of 10 or more). In contrast, the few particle manipulations that can still work effectively in high *Re* (on the order of 10 or more) flows rely on the elasticity of either DNA or HA solutions. In both types of biofluids, however, the value of *Wi* is still (at least) one order of magnitude different from that of *Re*. It therefore remains unknown for particle motions in microchannel non-Newtonian fluid flows with comparable elastic and inertial effects, i.e., $El \sim 1$. Moreover, the quantitative theoretical/numerical understanding and simulation of the experimentally observed particle behaviors are still largely lacking due to the complexity of the

Table 2
Summary of particle separation methods in microchannel non-Newtonian fluid flows.

Ref.	Channel structure	Channel dimension	Sheath flow	Fluid	Marker	Particle (d/μm)	Particle flow rate	Wi[a]	Re[a]
Nam et al. [121]	Straight square	50×50 μm^2	Yes	500 ppm PEO	Size	PS (1, 5) Blood cells	30 μl/h	12.7	0.81
Lim et al. [64]	Straight rectangular	100×50 μm^2	Yes	100 ppm PAA 500 ppm PEO	Size	PS (1, 10)	30 μl/h	3.04 1.29	0.51 0.54
Kang et al. [96]	Straight square	50[a] $\times$ 52 μm^2	Yes	5 ppm λ-DNA	Size	PS (1, 2.3, 4.5, 10.5)	100 μl/h	1256	5.72
Lu et al. [123]	Straight rectangular	50×25 μm^2 50×40 μm^2 50×100 μm^2	Yes	500–2000 ppm PEO	Size	PS (3, 10)	0.1–2 ml/h	7.2–144.7	0.17–3.4
Yang et al. [30]	Straight square	50×50 μm^2	No	250 ppm PEO 8% PVP	Size	PS (2.4, 5.9)	0.20 ml/h	8.04	0.37
Ahn et al. [124]	Straight square	50×50 μm^2	No	100–1000 ppm PEO	Size	PS (2.3, 4.5)	0.08–0.48 ml/h	0.96–25.6	0.1–1.37
Yuan et al. [125]	Straight rectangular, triangular side-wells	100×40 μm^2	No	1000 ppm PEO	Size	PS (3, 4.8, 10) Blood	20–80 μl/min	20.82–83.28	0.4–1.6
Nam et al. [126]	Straight cylindrical, 1st stage	43 μm dia.	No	8% PVP	Size	PS (5, 10) blood cells	0.06–30 μl/h	0.002–0.93	3.57e−6 to 1.78e−3
Nam et al. [127]	Straight cylindrical, 1st stage	50 μm dia.	No	0.1% HA	Size	MCF-7 cells Leukocytes	200 μl/min	1.8	27.4
Nam et al. [128]	Straight rectangular, 1st stage	25×250 μm^2	No	0.1% HA	Size	PS (2, 10) WBCs Malaria parasites	400 μl/min	2.8	53.9
Liu et al. [110]	Straight rectangular	100×50 μm^2 40×10 μm^2	No	2000 ppm PEO	Size	PS (1, 3, 5, 15) MCF-7, RBCs, *E. coli*	3 ml/h 0.1 ml/h	146.7 7.64	4.17 0.29
Li et al. [109]	Straight rectangular	50×25 μm^2	No	1000 ppm PEO	Size	PS (3, 5, 10)	0.3 ml/h	18.1	0.97
Liu et al. [28]	Spiral rectangular	30×4 μm^2	No	0.2–2% PEO in Tris-EDTA	Size	PS (0.1, 0.049) DNA	0.32–2.45 μl/h	0.09–0.67	<0.005
Lee et al. [112]	Spiral rectangular	100×25 μm^2	No	500–5000 ppm PEO	Size	PS (1.5, 5, 10)	50–750 μl/h	0.03–13.4	0.1–1
Lu et al. [129]	Straight rectangular	50×25 μm^2	Yes	1000 ppm PEO	Shape	PS (4.2, sphere & peanut)	5 μl/h	6.36	0.34
Lu et al. [130]	Straight rectangular	50×25 μm^2	No	1000 ppm PEO	Shape	PS (4.2, sphere & peanut)	150 μl/h	9.1	0.48
Yang et al. [131]	Straight square	75×75 μm^2	No	6.8% PVP in PBS	Stiffness	PS (6) RBCs, WBCs	0.16 ml/h	0.20	0.007
Del Giudice et al. [132]	Straight rectangular	100×50 μm^2	No	0.5% polyacrylamide	Magnetic	PS (10: magnetic; 6, 20: diamagnetic)	120 μl/h	De = 0.24	0.03
Kim et al. [133]	Straight square	50×50 μm^2	No	0.4% PEO 0.1 × EMG 408	Size	PS (5, 20: diamagnetic)	50 μl/h	1.41	0.03
Zhang et al. [134]	Straight rectangular	50×56 μm^2	No	1000 ppm PEO 0.1 × EMG 408	Size	PS (5, 13: diamagnetic)	15 μl/min	44.28	1.65

[a] Note: estimated based on the giving fluid properties if not provided in the paper.

Table 3
Summary of particle washing and stretching methods in microchannel non-Newtonian fluid flows.

Ref.	Manipulation	Channel structure	Channel dimension	Fluid	Particle (d in μm)	Particle flow rate	Wi[a]	Re[a]
Ha et al. [136]	Washing	H-shape rectangular	$30 \times 54\ \mu m^2$	0.01% λ-DNA in TE	PS (9.9, 2.0)	40 μl/min	3566	8.92
Yuan et al. [137]	Washing	Y-shape rectangular	$30 \times 50\ \mu m^2$	1000 ppm PEO	PS (4.8)	5 μl/min	52.22	0.35
Cha et al. [139]	Stretching	Cross-slot rectangular	$50 \times 50\ \mu m^2$	6.8 wt.% PVP in PBS	RBCs	160 μl/h	$De = 0.17$	<0.01
Bae et al. [140]	Stretching	Cross-slot rectangular	$50 \times 51.5\ \mu m^2$	6.8 wt.% PVP in PBS	CHO cell (13.4)	1500 μl/h	$Wi = 9.39$	0.13
Lim et al. [29]	Stretching	Straight square	$80 \times 80\ \mu m^2$	0.1% (w/v) HA	WBCs	20 ml/min	566	4422

[a] Note: estimated based on the giving fluid properties if not provided in the paper.

problem itself that requires the further development of both efficient algorithms and accurate constitutive equations. Other aspects that may be worthy of future studies include the migration of deformable particles in viscoelastic fluid flows through microchannels, and the integration of the passive flow-induced elasto-inertial force with an active externally-applied force for the manipulation of particles with desirable acoustic, electric or optical properties, etc.

References

[1] D.A. Ateya, J.S. Erickson, P.B. Howell Jr., L.R. Hilliard, J.P. Golden, F.S. Ligler, The good, the bad, and the tiny: a review of micro flow cytometry, Anal. Bioanal. Chem. 391 (2008) 1485–1498.
[2] X. Xuan, J. Zhu, C. Church, Particle focusing in microfluidic devices, Microfluid. Nanofluid. 9 (2010) 1–16.
[3] J. Nilsson, M. Evander, B. Hammarstrom, T. Laurell, Review of cell and particle trapping in microfluidic systems, Anal. Chim. Acta 649 (2009) 141–157.
[4] E.D. Pratt, C. Huang, B.G. Hawkins, J.P. Gleghorn, B.J. Kirby, Rare cell capture in microfluidic devices, Chem. Eng. Sci. 66 (2011) 1508–1522.
[5] N. Pamme, Continuous flow separations in microfluidic devices, Lab Chip 7 (2007) 1644–1659.
[6] A. Karimi, S. Yazdi, A.M. Ardekani, Hydrodynamic mechanisms of cell and particle trapping in microfluidics, Biomicrofluid 7 (2013) 021501.
[7] T.M. Squires, S.R. Quake, Microfluidics: fluid physics at the nanoliter scale, Rev. Mod. Phys. 77 (2005) 977–1026.
[8] E.K. Sackmann, A.L. Fulton, D.J. Beebe, The present and future role of microfluidics in biomedical research, Nature 507 (2014) 181–189.
[9] A. Groisman, M. Enzelberger, S. Quake, Microfluidic memory and control devices, Science 300 (2003) 955–958.
[10] J.J. Stickel, R.L. Powell, Fluid mechanics and rheology of dense suspensions, Annu. Rev. Fluid Mech. 37 (2005) 129–149.
[11] O.L. Hemmingera, P.E. Boukany, S.Q. Wang, L.J. Lee, Flow pattern and molecular visualization of DNA solutions through a 4:1 planar micro-contraction, J. Non-Newton. Fluid Mech. 165 (2010) 1613–1624.
[12] X. Hu, P.E. Boukany, O.L. Hemminger, L.J. Lee, The use of microfluidics in rheology, Macromol. Mater. Eng. 296 (2011) 308–320.
[13] C.J. Pipe, G.H. McKinley, Microfluidic rheometry, Mech. Res. Comm. 36 (2009) 110–120.
[14] C. Zhao, C. Yang, Electrokinetics of non-Newtonian fluids: a review, Adv. Colloid Interf. Sci. 201 (2013) 94–108.
[15] G. D'Avino, P.L. Maffettone, Particle dynamics in viscoelastic liquids, J. Non-Newton. Fluid Mech. 215 (2015) 80–104.
[16] G. D'Avino, F. Greco, P.L. Maffettone, Particle migration due to viscoelasticity of the suspending liquid and its relevance in microfluidic devices, Annu. Rev. Fluid Mech. 49 (2017) 341–360.
[17] T. Laurell, F. Petersson, A. Nilsson, Chip integrated strategies for acoustic separation and manipulation of cells and particles, Chem. Soc. Rev. 36 (2007) 492–506.
[18] M. Li, W. Li, J. Zhang, G. Alici, W. Wen, A review of microfabrication techniques and dielectrophoretic microdevices for particle manipulation and separation, J Phys. D 47 (2014) 063001.
[19] M. Hejazian, W. Li, N.T. Nguyen, Lab on a chip for continuous flow magnetic cell separation, Lab Chip 15 (2015) 959–970.
[20] A.A. Kayani, K. Khoshmanesh, S.A. Ward, A. Mitchell, K. Kalantar-Zadeh, Optofluidics incorporating actively controlled micro and nano-particles, Biomicrofluid 6 (2012) 031501.
[21] D. Di Carlo, Inertial microfluidics, Lab Chip 9 (2009) 3038–3046.
[22] D. Di Carlo, D. Irimia, R.G. Tompkins, M. Toner, Continuous inertial focusing, ordering, and separation of particles in microchannels, Proc. Natl. Acad. Sci. 104 (2007) 18892–18897.
[23] J.M. Martel, M. Toner, Inertial focusing in microfluidics, Annu. Rev. Biomed. Eng. 16 (2014) 371–396.
[24] H. Amini, W. Lee, D. Di Carlo, Inertial microfluidic physics, Lab Chip 14 (2014) 2739–2761.
[25] J. Zhang, S. Yan, D. Yuan, G. Alici, N.T. Nguyen, M.E. Warkiani, W. Li, Fundamentals and applications of inertial microfluidics: a review, Lab Chip 16 (2016) 10–34.
[26] J.Y. Kim, S.W. Ahn, S.S. Lee, J.M. Kim, Lateral migration and focusing of colloidal particles and DNA molecules under viscoelastic flow, Lab Chip 12 (2012) 2807–2814.
[27] I. De Santo, G. D'Avino, G. Romeo, F. Greco, P.A. Netti, P.L. Maffettone, Microfluidic Lagrangian trap for Brownian particles: three-dimensional focusing down to the nanoscale, Phys. Rev. Appl. 2 (2014) 064001.
[28] C. Liu, B. Ding, C. Xue, Y. Tian, G. Hu, J. Sun, Sheathless focusing and separation of diverse nanoparticles in viscoelastic solutions with minimized shear thinning, Anal. Chem. 88 (2016) 12547–12553.
[29] E.J. Lim, T.J. Ober, J.F. Edd, S.P. Desai, D. Neal, K.W. Bong, P.S. Doyle, G.H. McKinley, Mehmet Toner, Inertio-elastic focusing of bioparticles in microchannels at high throughput, Nat. Comm. 5 (2014) Article number: 4120.
[30] S. Yang, J.Y. Kim, S.J. Lee, S.S. Lee, J.M. Kim, Sheathless elasto-inertial particle focusing and continuous separation in a straight rectangular microchannel, Lab Chip 11 (2011) 266–273.
[31] M. Trofa, M. Vocciante, G. D'Avino, M.A. Hulsen, F. Greco, P.L. Maffettone, Numerical simulations of the competition between the effects of inertia and viscoelasticity on particle migration in Poiseuille flow, Comput. Fluid 107 (2015) 214–223.
[32] L.G. Leal, The motion of small particles in non-Newtonian fluids, J. Non-Newton. Fluid Mech. 5 (1979) 33–78.
[33] L.G. Leal, Particle motions in a viscous fluid, Annu. Rev. Fluid Mech. 12 (1980) 435–476.
[34] P. Brunn, The motion of rigid particles in viscoelastic fluids, J. Non-Newton. Fluid Mech. 7 (1980) 271–288.
[35] G.H. McKinley, Steady and transient motion of spherical particles in viscoelastic liquids, in: D. DeKee (Ed.), Transport Processes in Bubble, Drops, Particles, CRC Press, 2002, pp. 338–375.
[36] P.Y. Huang, D.D. Joseph, Effects of shear-thinning on migration of neutrally buoyant particles in pressure driven flow of Newtonian and viscoelastic fluids, J. Non-Newton. Fluid Mech. 90 (2000) 159–185.
[37] E.F. Lee, D.L. Koch, Y.L. Joo, Cross-stream forces and velocities of fixed and freely suspended particles in viscoelastic Poiseuille flow: perturbation and numerical analyses, J. Non-Newton. Fluid Mech. 165 (2010) 1309–1327.
[38] G. D'Avino, T. Tuccillo, P.L. Maffettone, F. Greco, M.A. Hulsen, Numerical simulations of particle migration in a viscoelastic fluid subjected to shear flow, Comput. Fluid 39 (2010) 709–721.
[39] M.M. Villone, G. D'Avino, M.A. Hulsen, F. Greco, P.L. Maffettone, Simulations of viscoelasticity-induced focusing of particles in pressure-driven micro-slit flow, J. Non-Newton. Fluid Mech. 166 (2011) 1396–1405.
[40] M.M. Villone, M.A. Hulsen, P.D. Anderson, P.L. Maffettone, Simulations of deformable systems in fluids under shear flow using an arbitrary Lagrangian Eulerian technique, Comput. Fluid 90 (2014) 88–100.
[41] G. Li, G.H. McKinley, A.M. Ardekani, Dynamics of particle migration in channel flow of viscoelastic fluids, J. Fluid Mech. 785 (2015) 486–505.
[42] M.M. Villone, F. Greco, M.A. Hulsen, P.L. Maffettone, Numerical simulations of deformable particle lateral migration in tube flow of Newtonian and viscoelastic media, J. Non-Newton. Fluid Mech. 234 (2016) 105–113.
[43] S. Gupta, W.S. Wang, S.A. Vanapalli, Microfluidic viscometers for shear rheology of complex fluids and biofluids, Biomicrofluid 10 (2016) 043402.
[44] E.W. Merrill, Rheology of blood, Physiol. Rev. 49 (1969) 863–888.
[45] O.K. Baskurt, H.J. Meiselman, Blood rheology and hemodynamics, Semin. Thromb. Hemost. 29 (2003) 435–450.
[46] L. Campo-Deaño, R.P. Dullens, D.G. Aarts, F.T. Pinho, M.S. Oliveira, Viscoelasticity of blood and viscoelastic blood analogues for use in polydymethylsiloxane in vitro models of the circulatory system, Biomicrofluid 7 (2013) 034102.
[47] M. Brust, C. Schaefer, R. Doerr, L. Pan, M. Garcia, P.E. Arratia, C. Wagner, Rheology of human blood plasma: viscoelastic versus Newtonian behavior, Phys. Rev. Lett. 110 (2013) 078305.
[48] R.G. Schipper, E. Silletti, M.H. Vingerhoeds, Saliva as research material: biochemical, physicochemical and practical aspects, Arch. Oral Bio. 52 (2007) 1114–1135.
[49] P.P. Bhat, S. Appathurai, M.T. Harris, M. Pasquali, G.H. McKinley, O.A. Basaran, Formation of beads-on-a-string structures during break-up of viscoelastic filaments, Nat. Phys. 6 (2010) 625–631.
[50] S.J. Haward, A. Jaishankar, M.S.N. Oliveira, M.A. Alves, G.H. McKinley, Extensional flow of hyaluronic acid solutions in an optimized microfluidic cross-slot device, Biomicrofluid 7 (2013) 044108.
[51] S.J. Haward, V. Sharma, J.A. Odell, Extensional opto-rheometry with biofluids and ultra-dilute polymer solutions, Soft Matt. 7 (2011) 9908–9921.

[52] L. Rems, D. Kawale, L.J. Lee, P.E. Boukany, Flow of DNA in micro/nanofluidics: from fundamentals to applications, Biomicrofluid 10 (2016) 043403.
[53] M.D. Graham, Fluid dynamics of dissolved polymer molecules in confined geometries, Annu. Rev. Fluid Mech. 43 (2011) 273–298.
[54] T.A. Waigh, Advances in the microrheology of complex fluids, Rep. Prog. Phys. 79 (2016) 074601.
[55] R.B. Bird, R.C. Armstrong, O. Hassager, Dynamics of Polymeric liquids: vol. 1, Fluid Mechanics; vol. 2: Kinetic Theory, Willey, 1977.
[56] R.G. Larson, The rheology of dilute solutions of flexible polymers: progress and problems, J. Rheol. 49 (2005) 1–70.
[57] I. Wong, C.M. Ho, Surface molecular property modifications for poly (dimethylsiloxane) (PDMS) based microfluidic devices, Microfluid. Nanofluid. 7 (2009) 291–306.
[58] M.S.N. Oliveira, M.A. Alves, F.T. Pinho, Microfluidic flows of viscoelastic fluids, in: R. Grigoriev (Ed.), Transport and Mixing in Laminar Flows: From Microfluidics to Oceanic Currents, first ed., Wiley-VCH, 2012.
[59] D.V. Boger, A highly elastic constant-viscosity fluid, J. Non-Newton. Fluid Mech. 3 (1977) 87–91.
[60] D.F. James, Boger fluids, Annu. Rev. Fluid Mech. 41 (2009) 129–142.
[61] L.E. Rodd, T.P. Scott, D.V. Boger, J.J. Cooper-White, G.H. McKinley, The inertio-elastic planar entry flow of low-viscosity elastic fluids in micro-fabricated geometries, J. Non-Newton. Fluid Mech. 129 (2005) 1–22.
[62] L.E. Rodd, J.J. Cooper-White, D.V. Boger, G.H. McKinley, Role of the elasticity number in the entry flow of dilute polymer solutions in micro-fabricated contraction geometries, J. Non-Newton. Fluid Mech. 143 (2007) 170–191.
[63] L.E. Rodd, D. Lee, K.H. Ahn, J.J. Cooper-White, The importance of downstream events in microfluidic viscoelastic entry flows: Consequences of increasing the constriction length, J. Non-Newton. Fluid Mech. 165 (2010) 1189–1203.
[64] H. Lim, J. Nam, S. Shin, Lateral migration of particles suspended in viscoelastic fluids in a microchannel flow, Microfluid. Nanofluid. 17 (2014) 683–692.
[65] R.B. Bird, J.M. Wiest, Constitutive equations for polymeric liquids, Annu. Rev. Fluid Mech. 27 (1995) 169–193.
[66] J.M. Dealy, Weissenberg and Deborah numbers—their definition and use, Rheol. Bull. 79 (2010) 14–18.
[67] B.P. Ho, L.G. Leal, Inertial migration of rigid spheres in two-dimensional unidirectional flows, J. Fluid Mech. 65 (1974) 365–400.
[68] L. Zeng, S. Balachandar, P. Fischer, Wall-induced forces on a rigid sphere at finite Reynolds number, J. Fluid Mech. 536 (2005) 1–25.
[69] L. Zeng, F. Najjar, S. Balachandar, P. Fischer, Forces on a finite-sized particle located close to a wall in a linear shear flow, Phys. Fluid 21 (2009) 033302.
[70] G. Segre, A. Silberberg, Radial particle displacements in Poiseuille flow of suspensions, Nature 189 (1961) 209–210.
[71] C. Liu, G. Hu, X. Jiang, J. Sun, Inertial focusing of spherical particles in rectangular microchannels over a wide range of Reynolds numbers, Lab Chip 15 (2015) 1168–1177.
[72] B. Chun, A.J.C. Ladd, Inertial migration of neutrally buoyant particles in a square duct: an investigation of multiple equilibrium positions, Phys. Fluid 18 (2006) 031704.
[73] E.S. Asmolov, The inertial lift on a spherical particle in a plane Poiseuille flow at large channel Reynolds number, J. Fluid Mech. 381 (1999) 63–87.
[74] D. Di Carlo, J.F. Edd, K.J. Humphry, H.A. Stone, M. Toner, Particle segregation and dynamics in confined flows, Phys. Rev. Lett. 102 (2009) 094503.
[75] C. Liu, C. Xue, J. Sun, G. Hu, A generalized formula for inertial lift on a sphere in microchannels, Lab Chip 16 (2016) 884–892.
[76] P.G.T. Saffman, The lift on a small sphere in a slow shear flow, J. Fluid Mech. 22 (1965) 385–400.
[77] J. Zhou, I. Papautsky, Fundamentals of inertial focusing in microchannels, Lab Chip 13 (2013) 1121–1132.
[78] J.P. Matas, J.F. Morris, E. Guazzelli, Lateral forces on a sphere, Oil Gas Sci. Technol. 59 (2004) 59–70.
[79] D. Yuan, C. Pan, J. Zhang, S. Yan, Q. Zhao, G. Alici, W. Li, Tunable particle focusing in a straight channel with symmetric semicircle obstacle arrays using electrophoresis-modified inertial effects, Micromachines 7 (2016) 195, http://dx.doi.org/10.3390/mi7110195.
[80] B.P. Ho, L.G. Leal, Migration of rigid spheres in a two-dimensional unidirectional shear flow of a second-order fluid, J. Fluid Mech. 76 (1976) 783–799.
[81] P.Y. Huang, J. Feng, H.H. Hu, D.D. Joseph, Direct simulation of the motion of solid particles in Couette and Poiseuille flows of viscoelastic fluids, J. Fluid Mech. 343 (1997) 73–94.
[82] M.M. Villone, G. D'Avino, M.A. Hulsen, F. Greco, P.L. Maffettone, Particle motion in square channel flow of a viscoelastic liquid: Migration vs. secondary flows, J. Non-Newton. Fluid Mech. 195 (2013) 1–8.
[83] H.A. Barnes, J.F. Hutton, K. Walters, An Introduction to Rheology, Elsevier, Amsterdam, 1989.
[84] J.A. Pathak, D. Ross, K.B. Migler, Elastic flow instability, curved streamlines, mixing in microfluidic flows, Phys. Fluid 16 (2004) 4028–4034.
[85] K.W. Seo, H.J. Byeon, H.K. Huh, S.J. Lee, Particle migration and single-line particle focusing in microscale pipe flow of viscoelastic fluids, RSC Adv. 4 (2014) 3512–3520.
[86] K.W. Seo, Y.J. Kang, S.J. Lee, Lateral migration and focusing of microspheres in a microchannel flow of viscoelastic fluids, Phys. Fluid 26 (2014) 063301.
[87] M.A. Tehrani, An experimental study of particle migration in pipe flow of viscoelastic fluids, J. Rheol. 40 (1996) 1057–1077.
[88] A.M. Leshansky, A. Bransky, N. Korin, U. Dinnar, Tunable nonlinear viscoelastic "focusing" in a microfluidic device, Phys. Rev. Lett. 98 (2007) 234501.
[89] S.A. Berger, L. Talbot, Flow in curved pipes, Annu. Rev. Fluid Mech. 15 (1983) 461–512.
[90] A.P. Sudarsan, V.M. Ugaz, Multivortex micromixing, Proc. Natl. Acad. Sci. USA 103 (2006) 7228–7233.
[91] D. Huh, W. Gu, Y. Kamotani, J.B. Grotgerg, S. Takayama, Microfluidics for flow cytometric analysis of cells and particles, Physiol. Meas. 26 (2005) R73–R98.
[92] T.D. Chung, H.C. Kim, Recent advances in miniaturized microfluidic flow cytometry for clinical use, Electrophoresis 28 (2007) 4511–4520.
[93] J. Godin, C. Chen, S.H. Cho, W. Qiao, F. Tsai, Y. Lo, Microfluidics and photonics for bio-system-on-a-chip: a review of advancements in technology towards a microfluidic flow cytometry chip, J. Biophoton. 1 (2008) 355–376.
[94] A. Karnis, H.L. Goldsmith, S.G. Mason, Axial migration of particles in Poiseuille flow, Nature 200 (1963) 159–160.
[95] A. Karnis, S.G. Mason, Particle motions in sheared suspensions. XIX. Viscoelastic media, Trans. Soc. Rheol. 10 (1966) 571–592.
[96] K. Kang, S.S. Lee, K. Hyun, S.J. Lee, J.M. Kim, DNA-based highly tunable particle focuser, Nat. Commun. (2013) 4 Article number 2567.
[97] D. Dannhauser, D. Rossi, F. Causa, P. Memmolo, A. Finizio, T. Wriedt, J. Hellmers, Y. Eremin, P. Ferraroc, P.A. Netti, Optical signature of erythrocytes by light scattering in microfluidic flows, Lab Chip 15 (2015) 3278–3285.
[98] G. D'Avino, G. Romeo, M.M. Villone, F. Greco, P.A. Netti, P.L. Maffettone, Single line particle focusing induced by viscoelasticity of the suspending liquid: theory, experiments and simulations to design a micropipe flow-focuser, Lab Chip 12 (2012) 1638–1645.
[99] G. Romeo, G. D'Avino, F. Greco, P.A. Netti, P.L. Maffettone, Viscoelastic flow-focusing in microchannels: scaling properties of the particle radial distributions, Lab Chip 13 (2013) 2802–2807.
[100] P.H. Chan, L.G. Leal, The motion of a deformable drop in a second-order fluid, J. Fluid Mech. 92 (1979) 131–170.
[101] R.G. Larson, Constitutive Equations for Polymer Melts and Solutions: Butterworths Series in Chemical Engineering, Butterworth-Heinemann, 2013.
[102] K.W. Seo, Y.R. Ha, S.J. Lee, Vertical focusing and cell ordering in a microchannel via viscoelasticity: applications for cell monitoring using a digital holographic microscopy, Appl. Phys. Lett. 104 (2014) 213702.
[103] A. Nikoubashman, N.A. Mahynski, A.H. Pirayandeh, A.Z. Panagiotopoulos, Flow-induced demixing of polymer-colloid mixtures in microfluidic channels, J. Chem. Phys. 140 (2014) 094903.
[104] M.P. Howard, A.Z. Panagiotopoulos, A. Nikoubashman, Inertial and viscoelastic forces on rigid colloids in microfluidic channels, J. Chem. Phys. 142 (2015) 224908.
[105] F. Del Giudice, G. Romeo, G. D'Avino, F. Greco, P.A. Netti, P.L. Maffettone, Particle alignment in a viscoelastic liquid flowing in a square-shaped microchannel, Lab Chip 13 (2013) 4263–4271.
[106] F.D. Giudice, G. D'Avino, F. Greco, P.A. Netti, P.L. Maffettone, Effect of fluid rheology on particle migration in a square-shaped microchannel, Microfluid. Nanofluid. 19 (2015) 95–104.
[107] H.Y. Song, S.H. Lee, R. Salehiyan, K. Hyun, Relationship between particle focusing and dimensionless numbers in elasto-inertial focusing, Rheol. Acta 55 (2016) 889–900.
[108] B. Kim, J.M. Kim, Elasto-inertial particle focusing under the viscoelastic flow of DNA solution in a square channel, Biomicrofluid 10 (2016) 024111.
[109] D. Li, X. Lu, X. Xuan, Viscoelastic separation of particles by size in straight rectangular microchannels: a parametric study for a refined understanding, Anal. Chem. 88 (2016) 12303–12309.
[110] C. Liu, C. Xue, X. Chen, L. Shan, Y. Tian, G. Hu, Size-based separation of particles and cells utilizing viscoelastic effects in straight microchannels, Anal. Chem. 87 (2015) 6041–6048.
[111] N. Xiang, Q. Dai, Z. Ni, Multi-train elasto-inertial particle focusing in straight microfluidic channels, Appl. Phys. Lett. 109 (2016) 134101.
[112] D.J. Lee, H. Brenner, J.R. Youn, Y.S. Song, Multiplex particle focusing via hydrodynamic force in viscoelastic fluids, Sci. Rep. 3 (2013) 3258.
[113] N. Xiang, X. Zhang, Q. Dai, J. Chen, K. Chen, Z. Ni, Fundamentals of elasto-inertial particle focusing in curved microfluidic channels, Lab Chip 16 (2016) 2626–2635.
[114] S. Cha, K. Kang, J.B. You, S.G. Im, Y. Kim, J.M. Kim, Hoop stress-assisted three-dimensional particle focusing under viscoelastic flow, Rheol. Acta 53 (2014) 927–933.
[115] D. Yuan, J. Zhang, S. Yan, C. Pan, G. Alici, N.T. Nguyen, W.H. Li, Dean-flow-coupled elasto-inertial three-dimensional particle focusing under viscoelastic flow in a straight channel with asymmetrical expansion–contraction cavity arrays, Biomicrofluid 9 (2015) 044108.
[116] D.R. Gossett, W.M. Weaver, A.J. Mach, S.C. Hur, H.T. Tse, W. Lee, H. Amini, D. Di Carlo, Label-free cell separation and sorting in microfluidic systems, Anal. Bioanal. Chem. 397 (2010) 3249–3267.
[117] P. Sajeesh, A.K. Sen, Particle separation and sorting in microfluidic devices: a review, Microfluid. Nanofluid. 17 (2014) 1–52.
[118] C.W. Iv Shields, C.D. Reyes, G.P. Lopez, Microfluidic cell sorting: a review of the advances in the separation of cells from debulking to rare cell isolation, Lab Chip 15 (2015) 1230–1249.
[119] G. Lee, S. Kim, K. Ahn, S. Lee, J.Y. Park, Separation and sorting of cells in microsystems using physical principles, J. Micromech. Microeng. 26 (2016) 013003.

[120] S. Yan, J. Zhang, D. Yuan, W. Li, Hybrid microfluidics combined with active and passive approaches for continuous cell separation, Electrophoresis 38 (2017) 238–249.
[121] J. Nam, H. Lim, D. Kim, H. Jung, S. Shin, Continuous separation of microparticles in a microfluidic channel via the elasto-inertial effect of non-Newtonian fluid, Lab Chip 12 (2012) 1347–1354.
[122] M. Yamada, M. Nakashima, M. Seki, Pinched flow fractionation: continuous size separation of particles utilizing a laminar flow profile in a pinched microchannel, Anal. Chem. 76 (2004) 5465–5471.
[123] X. Lu, X. Xuan, Continuous microfluidic particle separation via elasto-inertial pinched flow fractionation, Anal. Chem. 87 (2015) 6389–6396.
[124] S.W. Ahn, S.S. Lee, S.J. Lee, J.M. Kim, Microfluidic particle separator utilizing sheathless elasto-inertial focusing, Chem. Eng. Sci. 126 (2015) 237–243.
[125] D. Yuan, J. Zhang, R. Sluyter, Q. Zhao, S. Yan, G. Alicia, W. Li, Continuous plasma extraction under viscoelastic fluid in a straight channel with asymmetrical expansion–contraction cavity arrays, Lab Chip 16 (2016) 3919–3928.
[126] J. Nam, B. Namgung, C.T. Lim, J.E. Bae, H.L. Leo, K.S. Cho, S. Kim, Microfluidic device for sheathless particle focusing and separation using a viscoelastic fluid, J. Chromatogr. A 1406 (2015) 244–250.
[127] J. Nam, J.K.S. Tan, B.L. Khoo, B. Namgung, H.L. Leo, C.T. Lim, S. Kim, Hybrid capillary-inserted microfluidic device for sheathless particle focusing and separation in viscoelastic flow, Biomicrofluid 9 (2015) 064117.
[128] J. Nam, Y. Shin, J.K.S. Tan, Y.B. Lim, C.T. Lim, S. Kim, High-throughput malaria parasite separation using a viscoelastic fluid for ultrasensitive PCR detection, Lab Chip 16 (2016) 2086–2092.
[129] X. Lu, X. Xuan, Elasto-inertial pinched flow fractionation for continuous shape-based particle separation, Anal. Chem. 87 (2015) 11523–11530.
[130] X. Lu, L. Zhu, R.M. Hua, X. Xuan, Continuous sheath-free separation of particles by shape in viscoelastic fluids, Appl. Phys. Lett. 107 (2015) 264102.
[131] S. Yang, S.S. Lee, S.W. Ahn, K. Kang, W. Shim, G. Lee, K. Hyun, J.M. Kim, Deformability-selective particle entrainment and separation in a rectangular microchannel using medium viscoelasticity, Soft Matt. 8 (2012) 5011–5019.
[132] F. Del Giudice, H. Madadi, M.M. Villone, G. D'Avino, A.M. Cusano, R. Vecchione, M. Ventre, P.L. Maffettone, P.A. Netti, Magnetophoresis 'meets' viscoelasticity: deterministic separation of magnetic particles in a modular microfluidic device, Lab Chip 15 (2015) 1912–1922.
[133] M.J. Kim, D.J. Lee, J.R. Youn, Y.S. Song, Two step label free particle separation in a microfluidic system using elasto-inertial focusing and magnetophoresis, RSC Adv. 6 (2016) 32090–32097.
[134] J. Zhang, S. Yan, D. Yuan, Q. Zhao, S.H. Tan, N.T. Nguyen, W. Li, A novel viscoelastic-based ferrofluid for continuous sheathless microfluidic separation of nonmagnetic microparticles, Lab Chip 16 (2016) 3947–3956.
[135] F. Petersson, A. Nilsson, H. Jonsson, T. Laurell, Carrier medium exchange through ultrasonic particle switching in microfluidic channels, Anal. Chem. 77 (2005) 1216–1221.
[136] B. Ha, J. Park, G. Destgeer, J.H. Jung, H.J. Sung, Transfer of microparticles across laminar streams from non-Newtonian to Newtonian fluid, Anal. Chem. 88 (2016) 4205–4210.
[137] D. Yuan, J. Zhang, S. Yan, G. Peng, Q. Zhao, G. Alici, H. Du, W. Li, Investigation of particle lateral migration in sample-sheath flow of viscoelastic fluid and Newtonian fluid, Electrophoresis 37 (2016) 2147–2155.
[138] D.R. Gossetta, H.T.K. Tsea, S.A. Lee, Y. Ying, A.G. Lindgren, O.O. Yang, J. Rao, A. T. Clark, D. Di Carlo, Hydrodynamic stretching of single cells for large population mechanical phenotyping, Proc. Natl. Acad. Sci. USA 109 (2012) 7630–7635.
[139] S. Cha, T. Shin, S.S. Lee, W. Shim, G. Lee, S.J. Lee, Y. Kim, J.M. Kim, Cell stretching measurement utilizing viscoelastic particle focusing, Anal. Chem. 84 (2012) 10471–10477.
[140] Y.B. Bae, H.K. Jang, T.H. Shin, G. Phukan, T.T. Tran, G. Lee, W.R. Hwang, J.M. Kim, Microfluidic assessment of mechanical cell damage by extensional stress, Lab Chip 16 (2016) 96–103.